CANCELLATION OF REFLECTIONS DUE TO OBSTACLES IN AN ULTRA HIGH FREQUENCY TRANSMISSION LINE

Thesis by

David William Hagelbarger

In Partial Fulfilment of the Requirements for the Degree of Doctor of Philosophy

California Institute of Technology
Pasadena, California

1947

ABSTRACT

The theory of a new method of matching obstacle in ultra high frequency transmission lines, using the two wire transmission line analogy, is presented. The method is especially suited to the resonant cavity measurement technique, indicates a convenient form for tabulating data and reduces the matching conditions to their simplest form. The theory is extended to cover a frequency band rather than a single frequency and also to junctions between lines of different characteristic impedances. Experimental examples of each case are given as well as an example of the precision obtainable with the resonant cavity technique.

ACKNOWLEDGMENT

The author wishes to express his gratitude to Dr. William H. Pickering, Dr. Stanley C. Snowdon and Dr. Robert P. Dilworth for their guidance, counsel and aid in the preparation of this paper.

TABLE OF CONTENTS

CONTENTS

PART I

Introduction

The problem of finding the conditions for matching two obstacles placed in a wave guide was considered in an attempt to increase the usefulness of equivalent circuit data. It was felt that this data, originally taken to confirm theoretical computations, should be useful in designing actual systems. However, using the conventional equivalent circuit, the equations involved and the conditions for matching were so complicated as to perhaps account for the little use made of the data. A new notation was developed which would lend itself more readily to engineering practice. The solution of the matching problem in this notation, along with two experimental examples,is given in Part I.

The Canonical T-Section Parameters

A lossless obstacle placed in a wave guide or other microwave transmission line can be represented by a

4-terminal network containing purely reactive impedances.[1] We shall choose a symmetrical T-section*, but rather than the usual X_1 and X_2 (Fig. 1a), we shall use the canonical parameters S and T** (Fig. 1b) where:

$$S = X_1$$
$$T = X_1 + 2X_2 \qquad (1)$$

A considerable simplification of derivations, formulas, and calculations results from this substitution.

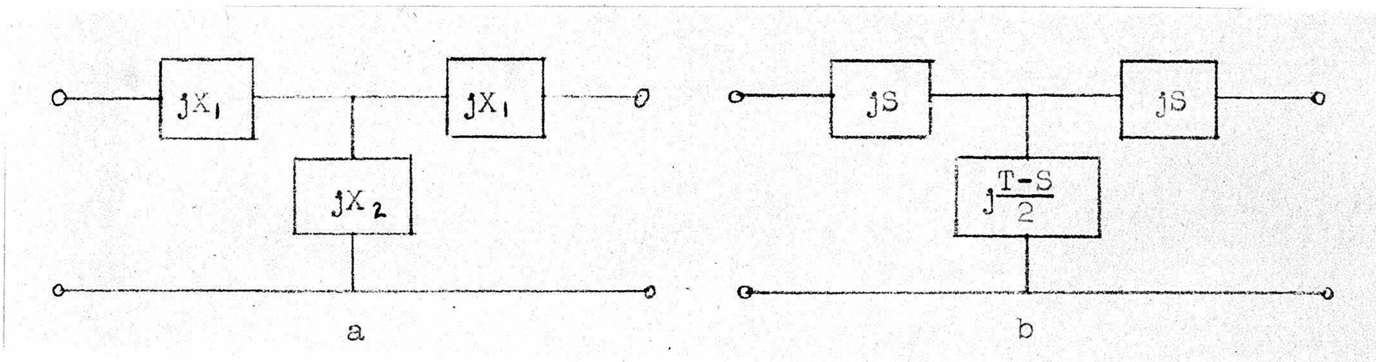

Fig. 1

In terms of these parameters:

$$Z_{sc} = j\,\frac{2TS}{T+S} \qquad (2)$$

$$Z_{oc} = j\,\frac{T+S}{2} \qquad (3)$$

$$Z_K = \sqrt{-TS} \qquad (4)$$

$$\cosh\Gamma = \frac{T+S}{T-S} \qquad (5)$$

---

[1]Numerical superscripts refer to bibliography.

*Any asymmetrical T-section is equivalent to a symmetrical section plus the proper length of line.

**These are closely related to the electrically equivalent lattice circuit.

Any T-section has two distinct representations as long as measurements across the series arms are not permitted. This is ordinarily the case. Using the canonical parameters, the one representation is obtained from the other by an interchange of S and T. In the following, nearly all the equations are invariant to such an interchange.

As we shall see later, S and T are measured directly by the resonant cavity method when the measurement is made so as to give the minimum error. Furthermore, the conditions for matching two obstacles are extremely simple in terms of S and T.

In what follows, unless otherwise stated, we shall measure all impedances in terms of the characteristic impedance. Using the dimensionless impedance $Z = \frac{z\ (\text{ohms})}{Z_K\ (\text{ohms})}$ is mathematically the same as letting $Z_K = 1$.

Conditions for Matching Two T-Sections

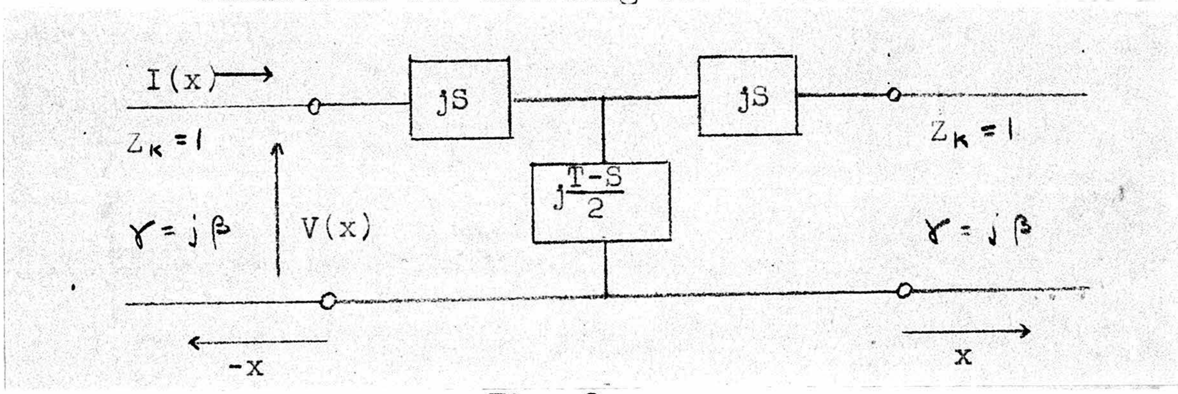

Fig. 2

If, in Fig. 2, we consider a wave advancing from the left with amplitude A, and being reflected with amplitude B and transmitted with amplitude C, it can be shown[2*] that the reflection coefficient

$$\frac{B}{A} = \cos(s-t)\, e^{-j(s+t)} \tag{6}$$

and the transmission coefficient

$$\frac{C}{A} = -j \sin(s-t)\, e^{-j(s+t)} \tag{7}$$

where:

$$T = \tan t \qquad S = \tan s \tag{8}$$

Further, the voltage standing wave ratio is given by

$$S.W.R. = \frac{1+|B/A|}{1-|B/A|} = \left\{ \begin{array}{ll} \cot^2 \frac{1}{2}(s-t), & -\frac{\pi}{2} < s-t < \frac{\pi}{2} \\ \tan^2 \frac{1}{2}(s-t), & \frac{\pi}{2} < s-t < \frac{3\pi}{2} \end{array} \right\} \tag{9}$$

If now we consider two obstacles separated by a distance L, the total reflection coefficient is given by [2**]

$$\frac{B}{A} = \frac{\cos(s_1-t_1)e^{-j(s_1+t_1)} - \cos(s_2-t_2)e^{-j[s_2+t_2+2(s_1+t_1)+2\beta L]}}{1-\cos(s_1-t_1)\cos(s_2-t_2)\,e^{-j(s_1+t_1+s_2+t_2+2\beta L)}} \tag{10}$$

In order to have the two obstacles match, we must have zero reflection, or B/A=0. This is fulfilled by either of the following two cases, both of which require that two conditions be satisfied; namely, that the reflection coefficients of the two obstacles have (1) equal amplitudes and (2) properly

* See Appendix C.
** See Appendix D.

chosen phases.

Case I
$$s_1 - t_1 = s_2 - t_2 + m\pi \tag{11}$$
$$\beta L = n\pi - (s_1 + t_2) = p\pi - (s_2 + t_1) \tag{12}$$

Case II*
$$s_1 - t_1 = -(s_2 - t_2) + m\pi \tag{13}$$
$$\beta L = n\pi - (s_1 + s_2) = p\pi - (t_1 + t_2) \tag{14}$$

$$m, n, p \text{ integers or zero}$$

Standing Wave Ratio Due to Small Mismatch

Let us now consider two obstacles which almost, but not entirely, satisfy these requirements. We wish to find the standing wave ratio. In Eq. 10, let:

$$s_1 - t_1 = s_2 - t_2 - \epsilon \tag{15}$$
$$\beta L = -s_1 - t_2 + \delta = -s_2 - t_1 + \delta + \epsilon \tag{16}$$

giving:

$$\frac{B}{A} = \cos(s_1 - t_1)e^{-j(s_1+t_1)} \left[\frac{1 - \frac{\cos(s_1 - t_1 + \epsilon)}{\cos(s_1 - t_1)} e^{-j(2\delta+\epsilon)}}{1 - \cos(s_1 - t_1)\cos(s_1 - t_1 + \epsilon)e^{-j(2\delta+\epsilon)}} \right] \tag{17}$$

Expanding and neglecting terms of second order and higher in ϵ and δ we get:

$$\frac{B}{A} \approx \frac{\cos(s_1 - t_1)e^{-j(s_1+t_1)}}{\sin^2(s_1 - t_1)} \left[\epsilon \tan(s_1 - t_1) + j(2\delta + \epsilon) \right] \tag{18}$$

---

* These are essentially the same because one can be obtained from the other by using the other representation ($S \leftrightarrows T$) for one of the obstacles.

Hence:

$$S.W.R. = \frac{1 + \cot(s_1 - t_1)\csc(s_1 - t_1)\sqrt{\epsilon^2 \tan^2(s_1 - t_1) + (2\delta + \epsilon)^2}}{1 - \cot(s_1 - t_1)\csc(s_1 - t_1)\sqrt{\epsilon^2 \tan^2(s_1 - t_1) + (2\delta + \epsilon)^2}} \tag{19}$$

Matching Over A Frequency Band, with Examples

It is usually desirable to match two obstacles over a frequency band rather than a single frequency. The two conditions

$$s_1 - t_1 = s_2 - t_2 \tag{20}$$

$$L = \frac{n\pi}{\beta} - \frac{s_1}{\beta} - \frac{t_2}{\beta} \tag{21}$$

must be satisfied throughout the range. Ordinarily s/β and t/β do not change rapidly with frequency and hence n must equal zero. When the standing wave ratio of the obstacles is not too large, $\tan(s-t) \gg 1$. This makes ϵ the more important term in Eq. 19 when ϵ and δ are of the same order of magnitude.

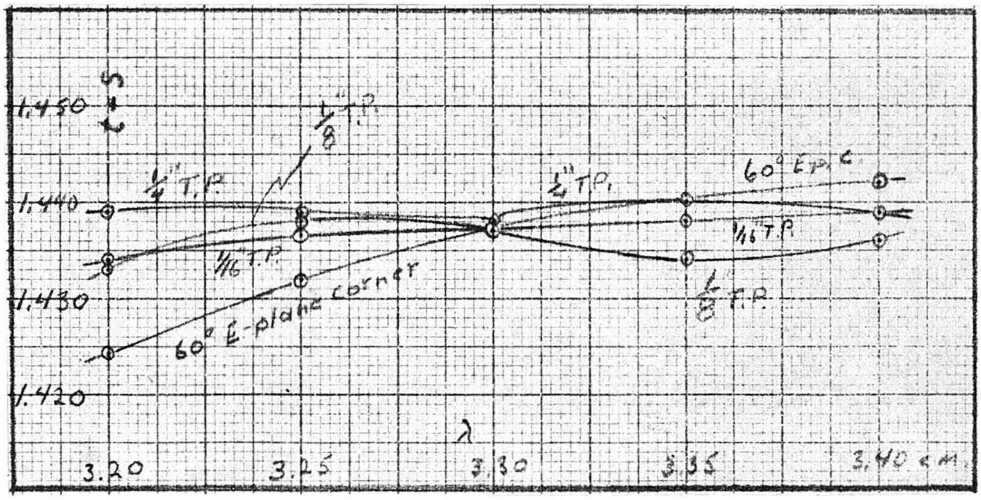

Fig. 3

	λ (cm)	3.20	3.25	3.30	3.35	3.40
E-Plane Corner	s-t	-1.424	-1.432	-1.437	-1.440	-1.446
	s	0.435	0.423	0.392	0.380	0.369
	t	-1.283	-1.287	-1.313	-1.321	-1.328
	s/β	0.122	0.123	0.118	0.117	0.117
1/16"T.P.	s-t	1.434	1.436	1.437	1.438	1.439
	s	-0.010	-0.002	-0.006	-0.004	-0.004
	t	-1.444	-1.438	-1.443	-1.442	-1.443
	s/β	-0.003	-0.000	-0.002	-0.001	-0.001
1/8" T.P.	s-t	1.433	1.438	1.437	1.434	1.436
	s	-0.020	-0.013	-0.015	-0.014	-0.014
	t	-1.453	-1.451	-1.452	-1.449	-1.450
	s/β	-0.006	-0.004	-0.004	-0.004	-0.004
1/4" T.P.	s-t	1.439	1.439	1.438	1.440	1.439
	s	-0.027	-0.023	-0.027	-0.024	-0.024
	t	-1.466	-1.462	-1.465	-1.464	-1.463
	s/β	-0.008	-0.007	-0.008	-0.007	-0.008

Table I

Fig. 3 and Table I give data for matching a 60 degree E-plane corner with 1/16", 1/8", and 1/4" tuning posts. The tuning posts were inserted in the guide just far enough in each case to give a good match at the center frequency, 3.30 cm. At first glance, it appears that the match would be fairly good for any of the three posts, with the 1/16" one having perhaps the slight edge on the others. Closer inspection shows a rather serious difficulty. When L is calculated from Eq. 21, letting n=0, it is found to come out negative. This is a physical impossibility and we must make n=1; that is, add 1/2 wavelength to L. The variation of this 1/2 wavelength with frequency produces a large effect which outweighs the small differences among the three tuning posts.

Fig. 4

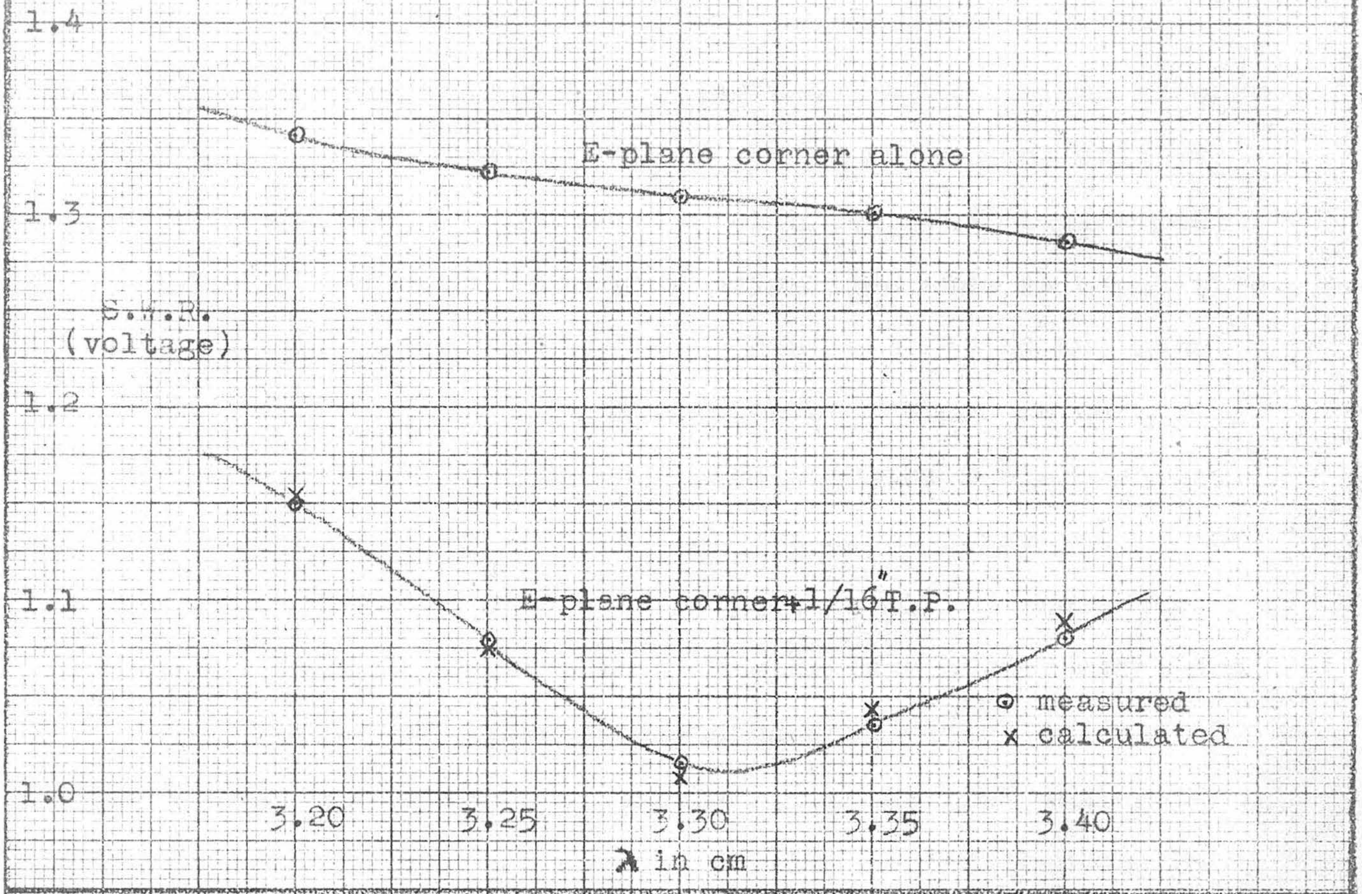
1.4
1.3
1.2
1.1
1.0
S.W.R.
(voltage)
E-plane corner alone
E-plane corner+1/16" T.P.
⊙ measured
x calculated
3.20
3.25
3.30
3.35
3.40
λ in cm

Fig. 5

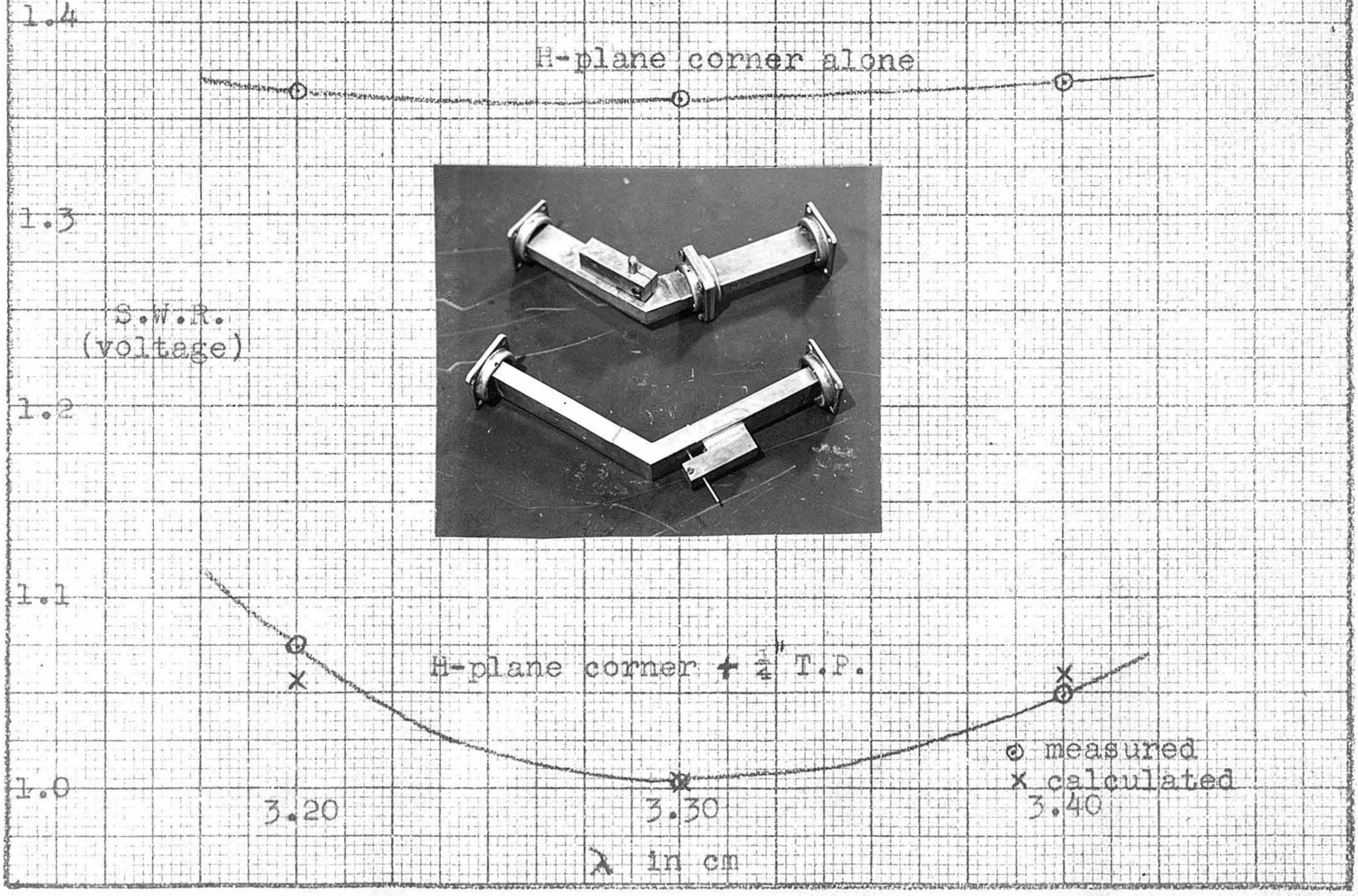
1.4
1.3
1.2
1.1
1.0
S.W.R.
(voltage)
H-plane corner alone
H-plane corner + 1/4" T.P.
⊙ measured
x calculated
3.20
3.30
3.40
λ in cm

Fig. 4 shows the measured standing wave ratios versus frequency for the 60 degree E-plane corner alone, and the calculated and measured values when matched with the 1/16" tuning post at 3.30 cm. Various other discontinuities such as capacitive change of guide height and tuning dent were tried but none of them had the large negative value of t which is necessary to give a positive length when used with the E-plane corner.

The 60 degree H-plane corner, however, lends itself more readily to matching with a tuning post. Fig. 5 shows the measured standing wave ratio of the H-plane corner alone and the calculated and measured standing wave ratios for the 60 degree H-plane corner when matched with the 1/4" tuning post. It may be noted that it is considerably better than the E-plane corner. The discrepancy between the calculated and measured values is probably due to the proximity effect. The separation between the two obstacles is only about 1/8 wavelength and it is likely that the higher modes are not sufficiently attenuated at this distance.

λ (cm)	3.20	3.25	3.30	3.35	3.40
60° E-Plane Corner					
Alone	1.341	1.322	1.309	1.300	1.286
With 1/16" T.P.					
Calculated	1.153	1.076	1.007	1.042	1.087
Measured	1.150	1.079	1.016	1.035	1.080
60° H-Plane Corner					
Alone	1.364		1.360		1.369
With 1/4" T.P.					
Calculated	1.056		1.003		1.058
Measured	1.074		1.004		1.049

Table II. Standing Wave Ratio (Voltage)

Table II gives the data plotted in Figs. 4 and 5.

Summarizing, in choosing a match for an obstacle, the three factors, in order of importance, are: (1) The matching obstacle should be chosen so that the length L is positive; (2) The values of s-t should agree as closely as possible throughout the range; and (3) The quantity $s_1/\beta + t_2/\beta$ should be a constant throughout the range.

Cavity Resonance Method of Measuring Equivalent Circuits

The above equivalent circuit parameters were measured by a variation of a technique first developed by C. Y. Meng, S. C. Snowdon, and D. W. Hagelbarger under the supervision of W. H. Pickering.[3] We form a cavity by short-circuiting each end of a wave guide containing the obstacle in question. Power is fed in through a small hole in one end, and the energy in the cavity is measured with a loosely coupled crystal detector probe inserted through a small hole in the cavity wall. The equivalent circuit parameters can then be calculated from the positions of the shorting plungers with respect to the reference planes of the obstacle. The equivalent circuit of the cavity is shown in Fig. 6.

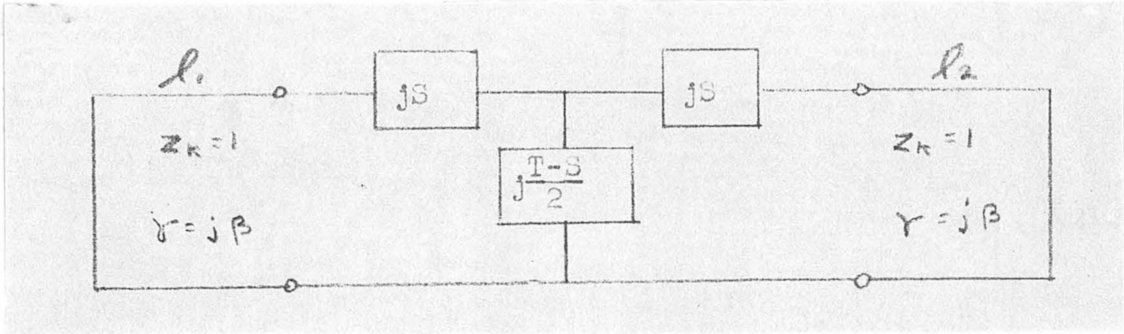

Fig. 6

The resonance condition is that the sum of the admittances across any point in the cavity must be zero, or, since the impedance of a short circuited line is $Z_i = jZ_K \tan\beta l_i$

$$\frac{1}{\tan\beta l_1 + S} + \frac{1}{\tan\beta l_2 + S} + \frac{2}{T - S} = 0 \tag{22}$$

This can be rewritten in several forms. For brevity, let:

$\beta l_i = \theta_i$, $\tan\beta l_i = \phi_i$

$$(T + S)(\phi_1 + \phi_2) + 2TS + 2\phi_1\phi_2 = 0 \tag{23a}$$

$$\frac{\phi_1 + T}{\phi_1 + S} = -\frac{\phi_2 + T}{\phi_2 + S} \tag{23b}$$

$$(T + S + 2\phi_2)(T + S + 2\phi_1) = (T - S)^2 \tag{23c}$$

From Eq. 23c it is easily seen that a plot of ϕ_1 vs. ϕ_2 gives a right hyperbola with $\phi_1 = -\frac{T+S}{2}$ and $\phi_2 = -\frac{T+S}{2}$ as asymptotes. Rotating the axes 45 degrees or plotting $\phi_1 + \phi_2$ vs. $\phi_1 - \phi_2$, we obtain curves symmetrical about $\phi_1 - \phi_2 = 0$, and hence at the maxima and minima $\phi_1 = \phi_2$ these points must be

$$\phi_1 = \phi_2 = -S$$

$$\phi_1 = \phi_2 = -T$$

A more convenient method of calculating S and T is to plot $\ell_1 + \ell_2$ vs. $\ell_1 - \ell_2$. In Eq. 23a, let:

$$\varphi_1 + \varphi_2 = \beta(\ell_1 + \ell_2) = 2\alpha$$
$$\varphi_1 - \varphi_2 = \beta(\ell_1 - \ell_2) = 2\beta'$$
$$A = \tan\alpha$$
$$B = \tan\beta'$$

giving:

$$(T+S)A(1+B^2) + TS(1-A^2B^2) + A^2 - B^2 = 0 \tag{24}$$

$$\frac{d\alpha}{d\beta'} = \frac{1+B^2}{1+A^2}\frac{dA}{dB} = \frac{2B(1+B^2)(A^2TS - A[T+S]+1)}{(1+A^2)[(T+S)(1+B^2) - 2AB^2TS + 2A]}$$

$$= \frac{2B(1+TS)}{[(T+S)(1+B^2) - 2AB^2TS + 2A]} \tag{25}$$

If $\frac{d\alpha}{d\beta'} = 0$ either $1 + TS = 0 \quad TS = -1$
or $B = 0$

If $TS = -1$, by Eq. 4 $Z_K = 1$ and the T-section is equivalent to a length of line giving $\ell_1 + \ell_2 = \text{constant}$. If B=0, then the curve has a maximum or minimum and $\ell_1 = \ell_2$, and from Eq. 24

$$A^2 + A(T+S) + TS = 0$$
$$A = -T \quad \text{or} \quad -S$$
$$\alpha = \frac{\beta(\ell_1 + \ell_2)}{2} = -t \quad \text{or} \quad -s$$

Thus at the maximum and minimum

$\beta\ell_1 = \beta\ell_2 = -t$ for one

and $\beta\ell_1 = \beta\ell_2 = -s$ for the other. (26)

Choice of Measurement Region to Give Minimum Error

Not only is the calculation of S and T simplest at the maximum and minimum points, but we shall now calculate the error $\sigma_{S,T}$ in S,T due to errors in the micrometer measurements of l_1 and l_2 and show that it has a minimum value at these points. S and T are to be measured, knowing that

$$(T+S)(\phi_1+\phi_2)+2TS+2\phi_1\phi_2=0\ , \tag{23a}$$

where $\phi_i = \tan\varphi_i$, by measuring two sets of values φ_1, φ_2 and φ_1', φ_2' and then solving the equations

$$(T+S)(\phi_1+\phi_2)+2TS+2\phi_1\phi_2=0 \tag{23a}$$

$$(T+S)(\phi_1'+\phi_2')+2TS+2\phi_1'\phi_2'=0 \tag{23a'}$$

for T and S. Given, that the error in φ_i, σ_{φ_i}, is a constant equal for all φ, what values of φ_1 and φ_1' (and therefore φ_2 and φ_2') should be chosen to give a minimum error in T and in S?

From symmetry considerations it would seem that these should be the same for both T and S. We will calculate the values for just S, then, as follows. Assuming a normal distribution, the standard deviation of S, σ_S, is given by:

$$\sigma_S^2=\left(\frac{\partial S}{\partial\varphi_1}\right)^2\sigma_{\varphi_1}^2+\left(\frac{\partial S}{\partial\varphi_2}\right)^2\sigma_{\varphi_2}^2+\left(\frac{\partial S}{\partial\varphi_1'}\right)^2\sigma_{\varphi_1'}^2+\left(\frac{\partial S}{\partial\varphi_2'}\right)^2\sigma_{\varphi_2'}^2 \tag{27}$$

We wish to minimize σ_S^2 with conditions that Eq. 23a and 23a' hold. This we do by solving the equations:

$$\frac{d\,\sigma_S^2}{d\,\varphi_1}=0 \tag{28}$$

$$\frac{d\,\sigma_S^2}{d\,\varphi_1'}=0 \tag{29}$$

for φ_1 and φ_1'.

Differentiating Eq. 23a and 23a', holding ϕ_2, ϕ_1' and ϕ_2' constant and eliminating $\frac{dT}{d\phi_1}$, we obtain

$$\left(\frac{dS}{d\phi_1}\right)_{\phi_2,\,\phi_1',\,\phi_2'} = \frac{\partial S}{\partial \phi_1} = \frac{(T + S + 2\phi_2)(\phi_1' + \phi_2' + 2S')}{2(T-S)(\phi_1 + \phi_2 - \phi_1' - \phi_2')}$$

Since: $$\frac{d\phi_1}{d\varphi_1} = \sec^2\varphi_1 = 1 + \phi_1^2$$

$$\frac{\partial S}{\partial \varphi_1} = \frac{(T + S + 2\phi_2)(\phi_1' + \phi_2' + 2S')}{2(T-S)(\phi_1 + \phi_2 - \phi_1' - \phi_2')}(1+\phi_1^2) \tag{30}$$

The other partials can be written by inspection:

$$\frac{\partial S}{\partial \varphi_2} = \frac{(T + S + 2\phi_1)(\phi_1' + \phi_2' + 2S')}{2(T-S)(\phi_1 + \phi_2 - \phi_1' - \phi_2')}(1+\phi_2^2) \tag{31}$$

$$\frac{\partial S'}{\partial \varphi_1'} = \frac{(T + S + 2\phi_2')(\phi_1 + \phi_2 + 2S')}{2(T-S)(\phi_1' + \phi_2' - \phi_1 - \phi_2)}(1+\phi_1'^2) \tag{32}$$

$$\frac{\partial S}{\partial \varphi_2'} = \frac{(T + S + 2\phi_1')(\phi_1 + \phi_2 + 2S')}{2(T-S')(\phi_1' + \phi_2' - \phi_1 - \phi_2)}(1+\phi_2'^2) \tag{33}$$

Substituting Eqs. 30, 31, 32, and 33 in Eq. 27, differentiating with respect to φ_1 and noting that:

$$\frac{d\phi_2}{d\phi_1} = -\frac{T + S + 2\phi_2}{T + S' + 2\phi_1}$$

We obtain, after simplification:

$$\frac{d\,\sigma_{S'}^2}{d\,\varphi_1} = \frac{(\phi_1' + \phi_2' + 2S')(1+\phi_1^2)}{(T-S')^2(\phi_1+\phi_2-\phi_1'-\phi_2')^3(T+S'+2\phi_1)} \Big\{(T+S'+2\phi_2)^2 \times$$
$$(\phi_1' + \phi_2' + 2S')(1+\phi_1^2)\left[(\phi_1+\phi_2-\phi_1'-\phi_2')(\phi_1^2+\phi_1\{T+S'\}-1)\right.$$
$$\left.-(\phi_1-\phi_2)(1+\phi_1^2)\right] - (T+S'+2\phi_1)^2(\phi_1'+\phi_2'+2S)\times$$
$$(1+\phi_2^2)\left[(\phi_1+\phi_2-\phi_1'-\phi_2')(\phi_2^2+\phi_2\{T+S'\}-1)\right.$$
$$\left.+(\phi_1-\phi_2)(1+\phi_2^2)\right] - (T+S'+2\phi_2')^2(\phi_1+\phi_2+2S')\times$$
$$(1+\phi_1'^2)^2(\phi_1-\phi_2)(1+\phi_1^2)^2 - (T+S'+2\phi_1')^2\times$$
$$(\phi_1+\phi_2+2S')(1+\phi_2'^2)^2(\phi_1-\phi_2)(1+\phi_1^2)^2\Big\} \tag{34}$$

$\frac{d\,\sigma_{S'}^2}{d\,\varphi_1'}$ can be written from Eq. 34 by interchanging ϕ_1 and ϕ_1' and interchanging ϕ_2 for ϕ_2'. We see by inspection that

$$\phi_1 = \phi_2 = -T \qquad \text{and} \qquad \phi_1' = \phi_2' = -S' \tag{35}$$

are solutions of Eqs. 23a, 23a', 28 and 29 simultaneously.

To show that these solutions are minima, we compute and evaluate the second derivatives, getting:

$$\left(\frac{d^2\sigma_{S'}^2}{d\,\varphi_1^2}\right)_{\substack{\phi_1=\phi_2=-T\\ \phi_1'=\phi_2'=-S'}} = 0$$

$$\left(\frac{d^2\sigma_{S'}^2}{d\,\varphi_1'^2}\right)_{\substack{\phi_1=\phi_2=-T\\ \phi_1'=\phi_2'=-S'}} = \frac{2(1+S^2)^2}{(T-S')^2}\left[(T+S')^2+(1+TS')^2+2+2T^2S'^2\right]$$

The first is zero, since $\sigma_{S'}^2$ is independent of φ_1, and the second is always positive.

If Eqs. 35 are satisfied,

$$\sigma_{S}^{2} = 0\cdot\sigma_{\varphi_1}^{2} + 0\cdot\sigma_{\varphi_2}^{2} + (-1)^2\sigma_{\phi_1'}^{2} + (-1)^2\sigma_{\phi_2'}^{2}$$
$$= 2(1+S^2)^2\sigma_{\varphi}^{2} \qquad (36)$$

From symmetry considerations, the solutions for

$$\frac{d\sigma_T^2}{d\varphi_1} = 0 \qquad \frac{d\sigma_T^2}{d\varphi_1'} = 0$$

are

$$\phi_1 = \phi_2 = -T \qquad \phi_1' = \phi_2' = -S$$

and

$$\sigma_T^2 = \sigma_{\phi_1}^2 + \sigma_{\phi_2}^2 + 0\cdot\sigma_{\phi_1'}^2 + 0\cdot\sigma_{\phi_2'}^2 \qquad (37)$$
$$= 2(1+T^2)^2\sigma_{\varphi}^2$$

In actual practice, the sum of the micrometer readings R_1+R_2 is plotted against R_1. Since R_1+R_2 differs from $\ell_1+\ell_2$ only by a constant, this curve will have its maximum and minimum in the same regions. Also, since only the values of the maximum and minimum are required, it is immaterial whether the data is plotted against R_1 or R_1-R_2. The constant is determined by obtaining resonance in the guide without the obstacle present. It is called the calibration sum, $(R_1+R_2)_S$, and its constancy is a measure of the uniformity of the test section and also the disturbing effect of the probe.

Description of Frequency Modulated System

The system shown in Figs. 7 and 8, while not capable of the highest possible absolute precision, lends itself to fairly rapid measurements with good relative precision and ease of changing frequency. Since the system shows the complete resonance curve, the disturbing effect of the probe in the test cavity and the uniformity of the oscillator throughout the resonant range can be quickly checked. It is essentially a method of comparing the resonant frequency of the test cavity with the standard cavity. The 723 A/B klystron is frequency modulated with a 60 ~ triangular voltage applied to the reflector. If the tube is properly loaded, the frequency modulation is linear and the amplitude modulation is small. The standard cavity is an absorption type wavemeter with a high Q. It is coupled to the system through an attenuator and tuning section so as to absorb energy at its resonant frequency. The test section

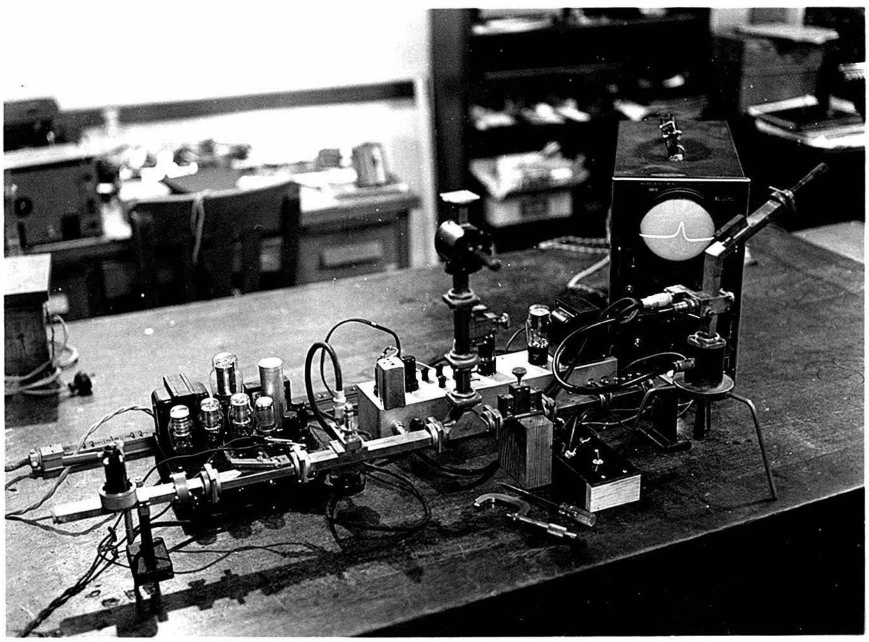

Fig. 7

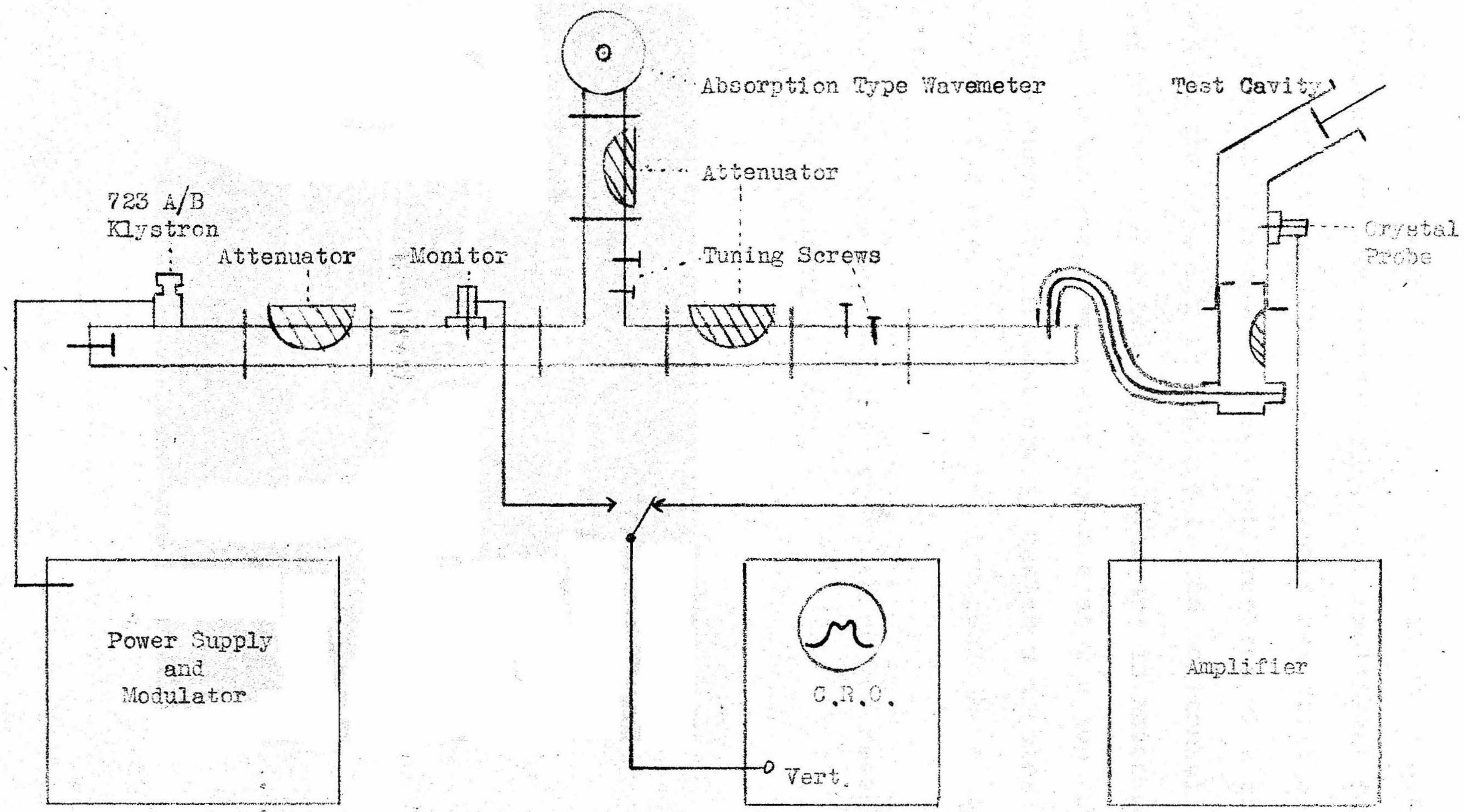

SCHEMATIC DIAGRAM OF FREQUENCY MODULATED SYSTEM

Fig. 8

is coupled to the system through its hollow input plunger and the crystal probe is connected through amplifiers to the vertical deflecting plates of a cathode ray oscilloscope. A 60-cycle sawtooth voltage synchronized with the modulation on the klystron is applied to the horizontal deflecting plates. When the two cavities are in resonance, the dip due to the standard cavity appears at the top of the resonance curve of the test cavity making a double-peaked curve. For exact resonance the two peaks have the same height.

Fig. 9 shows the test section approaching the resonant frequency of the standard cavity.

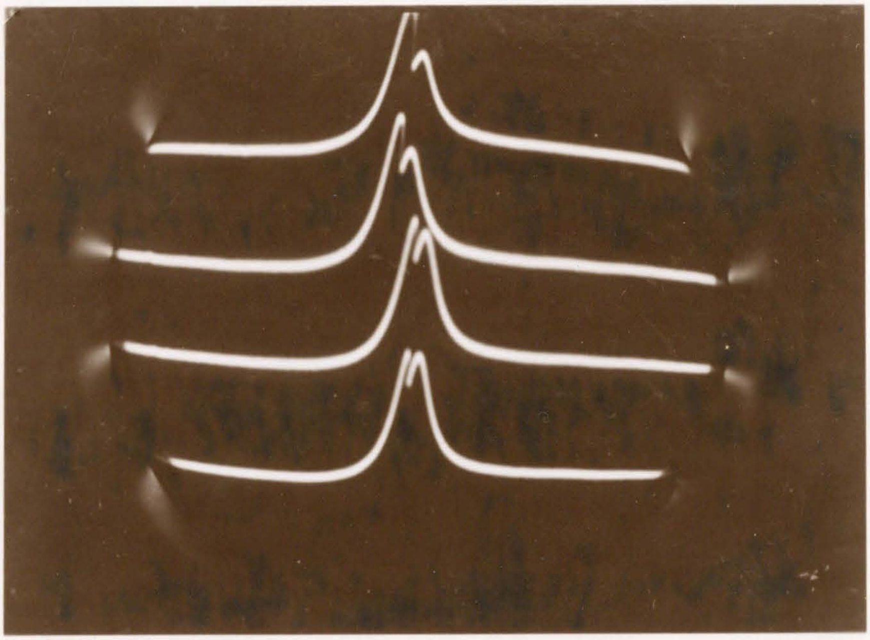

Fig. 9

The curves, reading from top to bottom, are .0010,

.0005, .0001, and .0000 inches away from resonance. The total length of the cavity was about $5\frac{1}{2}$ inches and a displacement of .0001 inch is easily distinguished.

The effect of the probe on the resonant frequency of the test cavity is illustrated in Fig. 10.

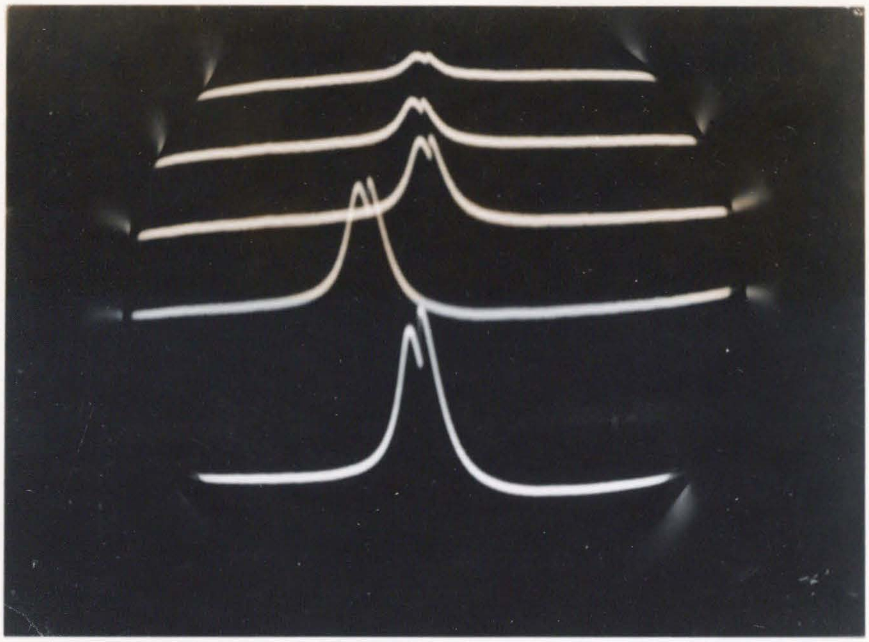

Fig. 10

The depth of penetration of the .010-inch diameter probe into the cavity is, reading from top to bottom, .015, .020, .025, .030, and .035 inches. Only in the last case does it affect the resonance frequency appreciably (the horizontal displacement of the curves is due to variation of the synchronizing voltage and is not pertinent).

In Fig. 11, the upper curve is the resonance curve of the test cavity, while the lower curve shows the energy in the main part of the system which is essentially constant over the range being swept. It is obtained from a monitoring probe in the guide between the oscillator and the standard cavity. It is extremely useful when changing frequency, and a switch is provided for quickly connecting either it or the test cavity to the oscilloscope.

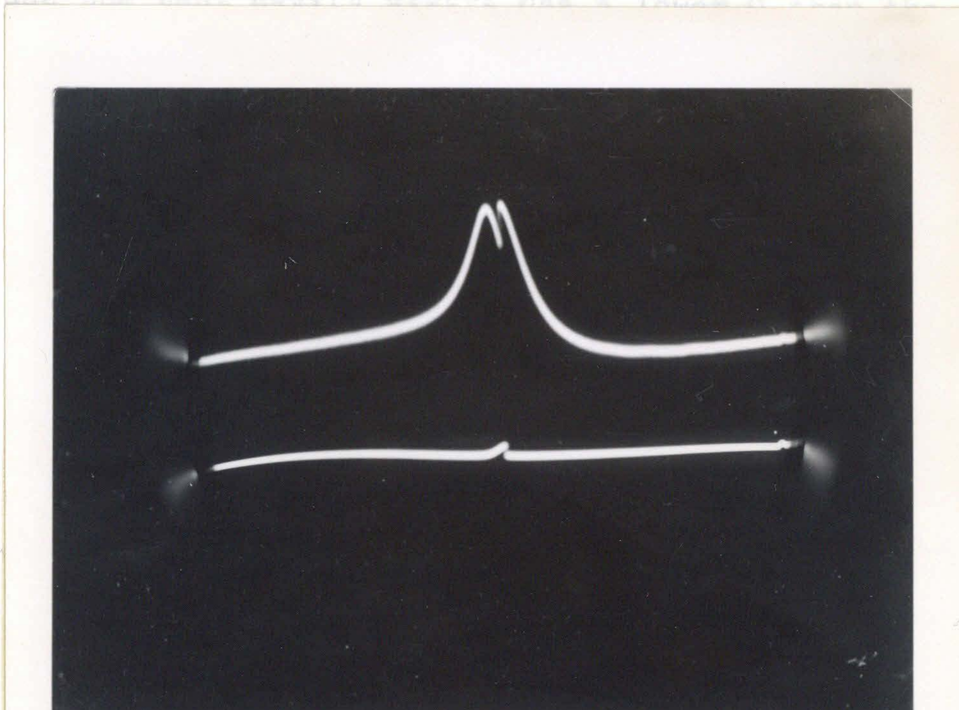

Fig. 11

An interesting effect is shown in Fig. 12. The resonant frequencies of the cavities appear to be slightly different when the frequency of the oscillator is increasing instead of decreasing. It was found that this was not due to delay in the wave guide system or poor low frequency response of amplifiers. When a frequency modulated signal is applied, one would expect a shifting of the resonance curve which is proportional to the Q of the cavity, since it requires approximately Q cycles for the cavity to reach a steady state. Because the test cavity always has a lower Q than the

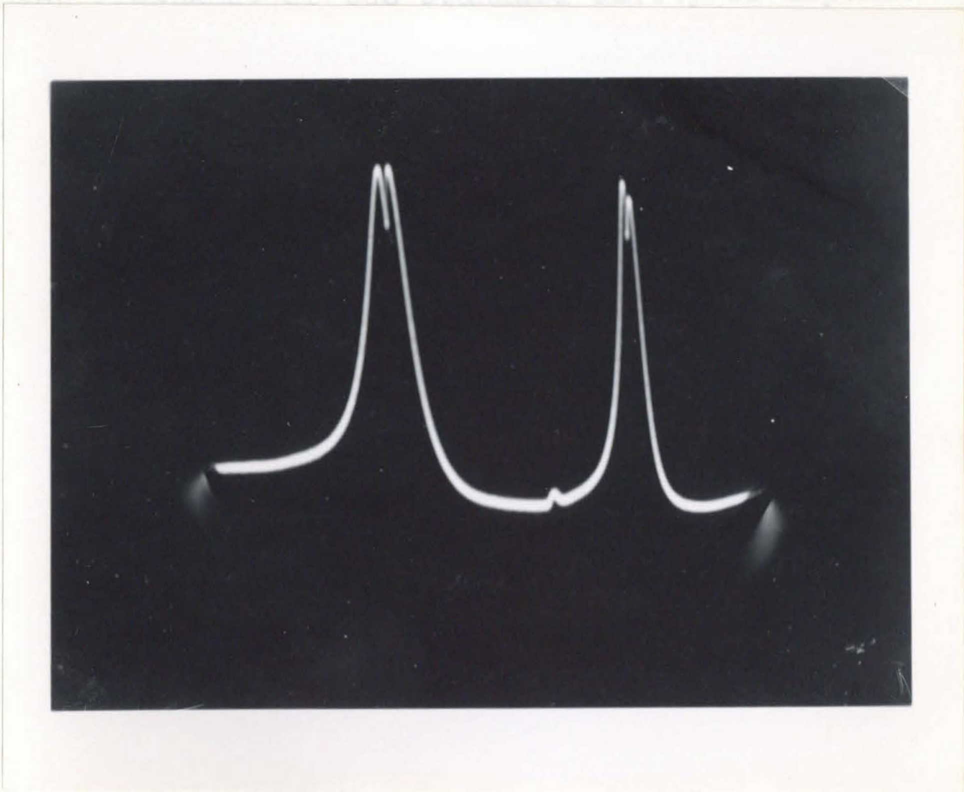

Fig. 12

standard cavity, the two will be shifted different amounts and hence, if the resonant frequencies appear the same when the frequency is increasing, they must appear off by twice the difference in the shifts when the frequency is decreasing. Care was taken to always use the same one of the two resonance curves during a series of measurements.

Sources of Errors

Perhaps the chief source of errors is the fact that the resonant frequency of the standard cavity is dependent on its coupling to the system. The 723 A/B tube is hardly powerful enough. Hence, at times it is necessary to couple the cavities too closely. Readings may be repeated to .0001 inch if the setup is not disturbed. However, if it is torn down and reassembled, the discrepancy may be as high as .0005 inches.

PART II

Extension of Matching Technique to a Four Terminal Network Between Lines With Different Characteristics

It is not possible to measure the characteristic impedance of a transmission line using a resonant cavity technique with purely reactive elements. This is because the determination of the characteristic impedance requires the measurement of a voltage-to-current ratio and the resonant cavity method merely locates positions on the transmission line where the voltage is zero. However, it is not necessary to know the characteristic impedances in order to get maximum power transfer across the junction between two lines; that is, to eliminate reflections from the junctions.

In Fig. 13 we have two different semi-infinite transmission lines whose junction is represented by the T-section

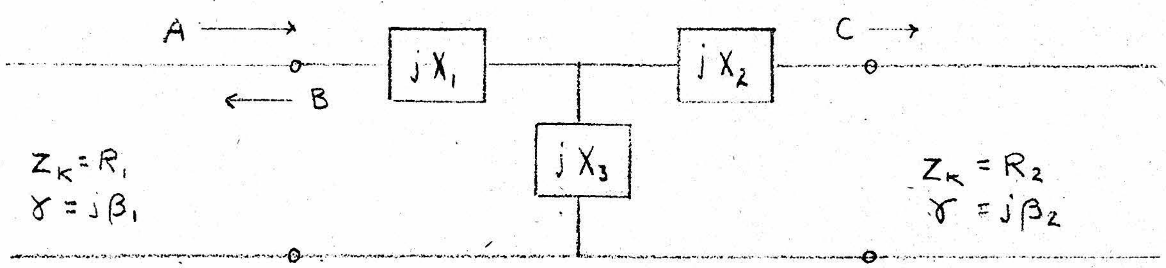

Fig. 13

shown. A wave of amplitude A is advancing from the left and is reflected with amplitude B and transmitted with amplitude C. The reflection coefficient B/A is given by:

$$\frac{B}{A} = \frac{Z_K - Z_R}{Z_K + Z_R} = \frac{R_1 - jX_1 - \dfrac{jX_3(R_2 + jX_2)}{R_2 + jX_2 + jX_3}}{R_1 + jX_1 + \dfrac{jX_3(R_2 + jX_2)}{R_2 + jX_2 + jX_3}} \tag{38}$$

Setting $\frac{B}{A} = 0$, we have:

$$(R_1 - jX_1)(R_2 + jX_2 + jX_3) - jX_3(R_2 + jX_2) = 0$$

from which

$$R_1R_2 + X_1X_2 + X_2X_3 + X_3X_1 = 0 \tag{39}$$

$$R_1(X_2 + X_3) - R_2(X_1 + X_3) = 0 \tag{40}$$

If we form a resonant cavity with portions of the same lines and T-section (Fig. 14), the resonant equation is:

$$\frac{1}{jX_1 + jR_1 \tan\beta_1 l_1} + \frac{1}{jX_2 + jR_2 \tan\beta_2 l_2} + \frac{1}{jX_3} = 0$$

or

$$R_1 R_2 \tan\beta_1 l_1 \tan\beta_2 l_2 + (X_2 + X_3) R_1 \tan\beta_1 l_1 + (X_1 + X_3) R_2 \tan\beta_2 l_2 + X_1 X_2 + X_2 X_3 + X_3 X_1 = 0 \tag{41}$$

Let us further require that $\beta_1 l_1 + \beta_2 l_2 = \text{const} = \cot^{-1} K$ (42)

Then:

$$\cot(\beta_1 l_1 + \beta_2 l_2) = K$$

$$\tan\beta_1 l_1 \tan\beta_2 l_2 + K \tan\beta_1 l_1 + K \tan\beta_2 l_2 - 1 = 0 \tag{43}$$

Now Eqs. 41 and 43 must hold simultaneously. Hence:

$$\frac{(X_2 + X_3) R_1}{X_1 X_2 + X_2 X_3 + X_3 X_1} = \frac{(X_1 + X_3) R_2}{X_1 X_2 + X_2 X_3 + X_3 X_1} = -K \tag{44}$$

$$\frac{R_1 R_2}{X_1 X_2 + X_2 X_3 + X_3 X_1} = -1 \tag{45}$$

But these are the conditions for zero reflection (Eqs. 39 and 40). Hence, Eq. 42 is the condition for which we are looking.

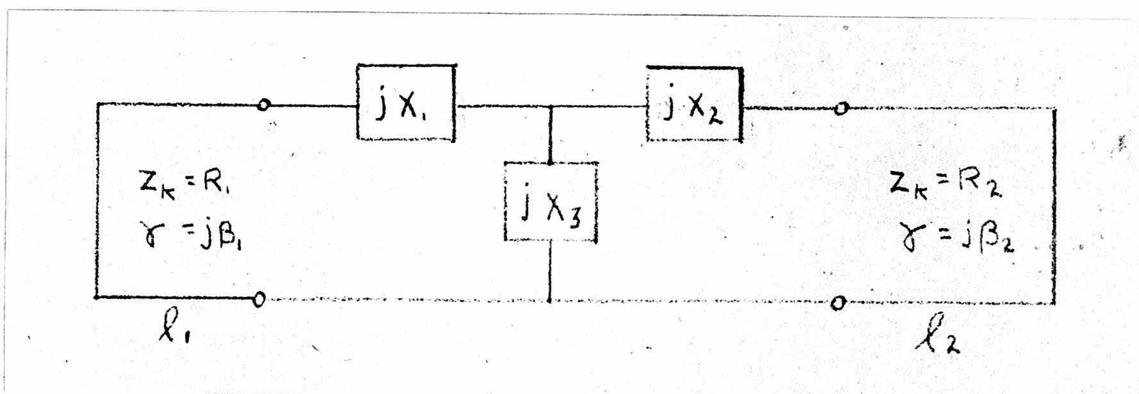

Fig. 14

This means that if we wish to match a junction such as Fig. 13, we may assume that the two characteristic impedances are both equal to unity, say, and measure the junction in the cavity of Fig. 14. If we calculate, using this assumption, the matching T-section according to the method outlined in Part I, then an obstacle will match the junction providing it gives the proper T-section when measured in the same transmission line as the one in which it is to be inserted. For example, suppose we have two wave guides of different dimensions meeting as in Fig. 15. We form a resonant cavity by inserting shortcircuiting plungers.

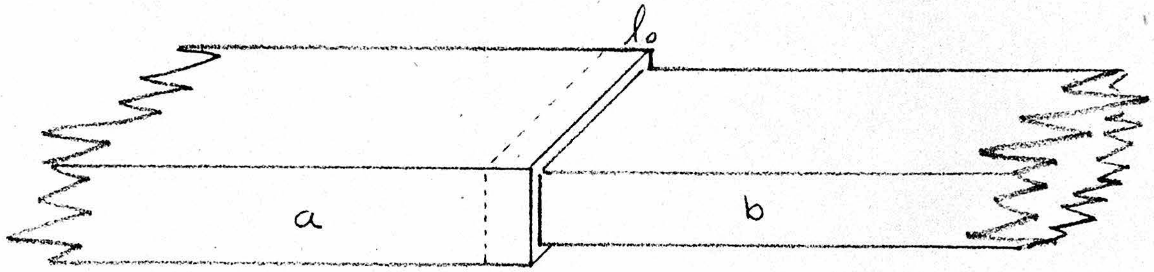

Fig. 15

From the resonance curve, taking into account the two β 's but assuming the Z_K 's are both unity, we find the junction behaves as a symmetrical T-section (see p. 35 $\ell_0 = \vartheta/\beta_a$) about the dotted line, a distance ℓ_0 from the physical junction, and has values s_j and t_j. To match it, we find an obstacle which, when measured in guide a, has T-section parameters s_a and t_a such that $s_a - t_a = -s_j + t_j$

We place this in guide a at a distance $\ell = \dfrac{-s_a - s_j}{\beta_a}$ from the dotted line, as shown in Fig. 16. We might equally

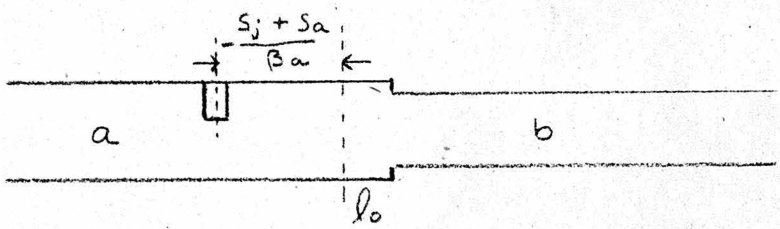

Fig. 16

well have found an object which, when measured in guide b, gave values s_b and t_b such that $s_b - t_b = -s_j + t_j$ and then placed it in guide b at a distance $\ell = -\dfrac{s_b + s_j}{\beta_b} + \left(1 - \dfrac{\beta_a}{\beta_b}\right)\ell_o$

as shown in Fig. 17.

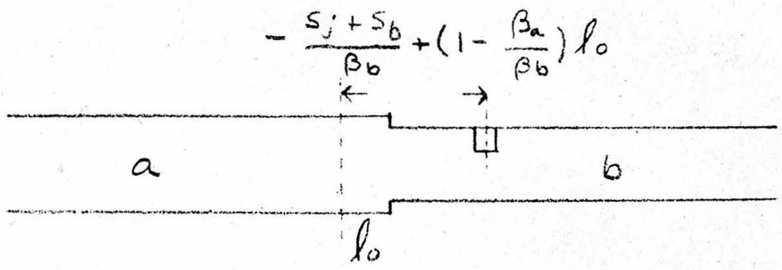

Fig. 17

Representation and Measurement of the Equivalent Circuit of The Junction Between Two Transmission Lines With Different Characteristics

Consider the junction formed by a coax line passing symmetrically through a wave guide so that the coax is parallel to the electric field in the guide (Fig. 18). We shall show that 5 parameters are required in the equivalent circuit of this junction.

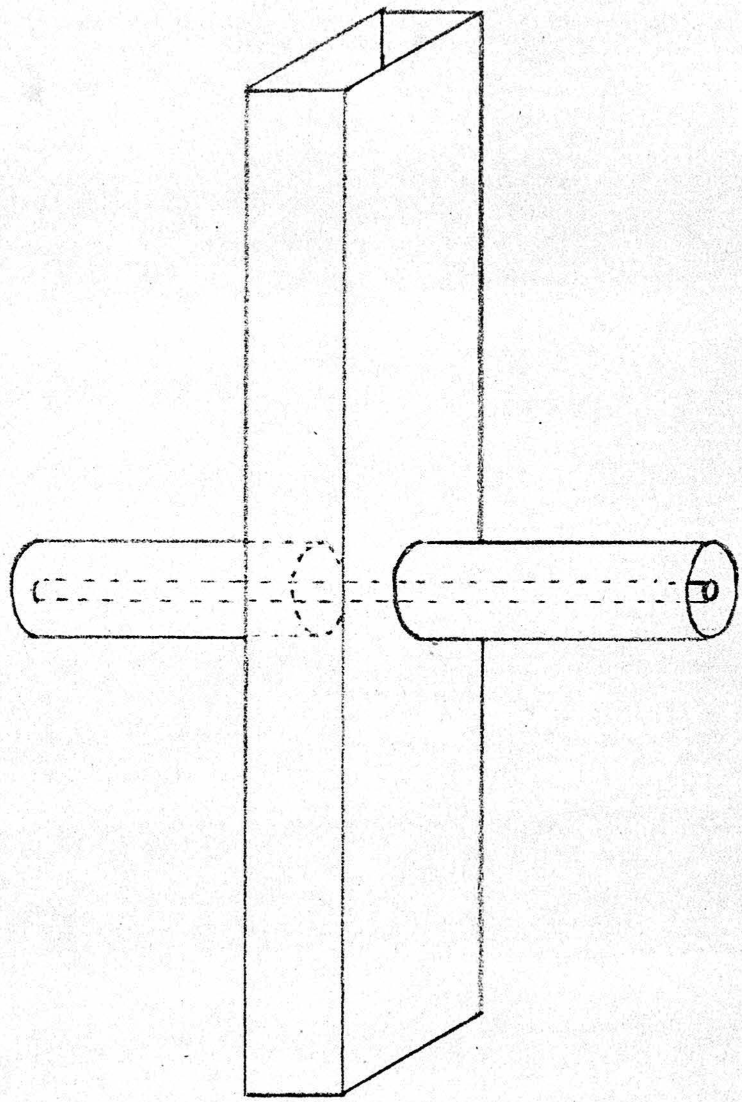

Fig. 18

A general 8-terminal black box (Fig. 19) has 4 independent voltages and 4 independent currents which are related by the following system of equations:

$$
\begin{aligned}
E_1 &= I_1 Z_{11} + I_2 Z_{12} + I_3 Z_{13} + I_4 Z_{14} \\
E_2 &= I_1 Z_{21} + I_2 Z_{22} + I_3 Z_{23} + I_4 Z_{24} \\
E_3 &= I_1 Z_{31} + I_2 Z_{32} + I_3 Z_{33} + I_4 Z_{34} \\
E_4 &= I_1 Z_{41} + I_2 Z_{42} + I_3 Z_{43} + I_4 Z_{44}
\end{aligned}
\qquad (46)
$$

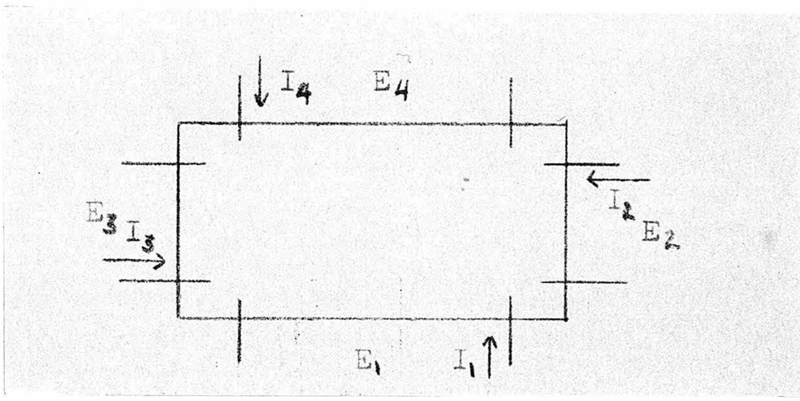

Fig. 19

Of the 16 coefficients in Eq. 46, only 10 are different, since $Z_{ik} = Z_{ki}$ by the reciprocity theorem. Imposing the symmetry properties of the coax-to-guide junction, namely the two coax arms may be interchanged and the two guide arms may be interchanged, we are left with just 5 independent impedances.

$$
\begin{aligned}
&Z_{14} \\
&Z_{23} \\
&Z_{11} = Z_{44} \\
&Z_{22} = Z_{33} \\
&Z_{12} = Z_{13} = Z_{24} = Z_{34}
\end{aligned}
\qquad (47)
$$

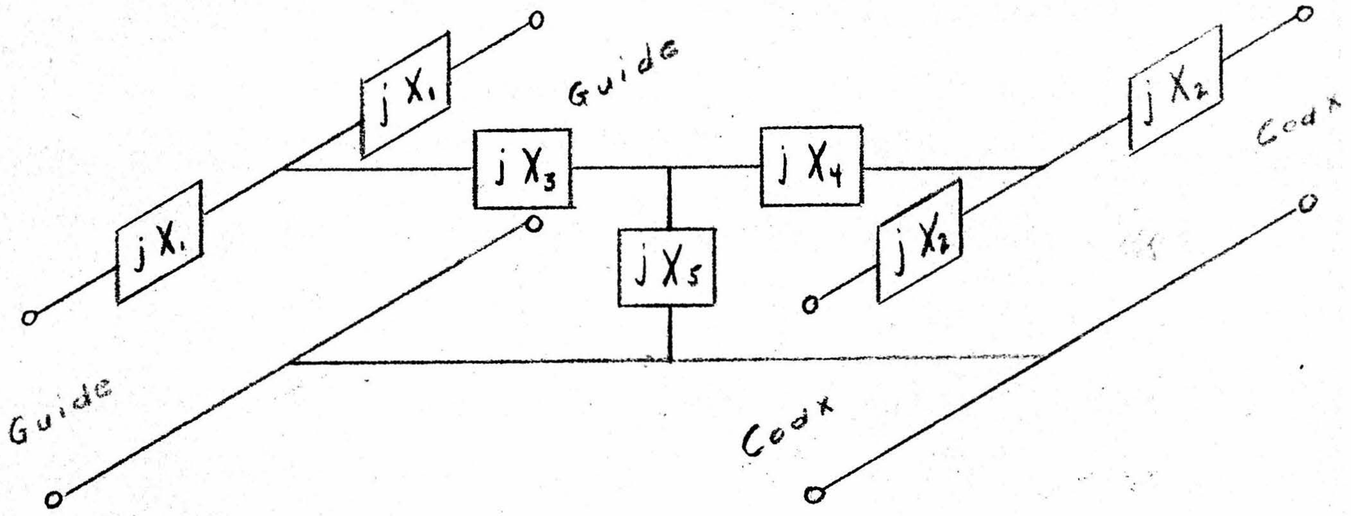

Fig. 20

The circuit of Fig. 20 is convenient to measure using the resonant cavity method. Since this circuit contains the 5 necessary parameters, we may arbitrarily equate the characteristic impedances of the guide and coax. Dividing by this common characteristic impedance gives us dimensionless impedances. The equivalent circuit will then predict completely the behavior of the junction, providing only impedances measured in the coax system are connected to the coax arms and impedances measured in the guide to the

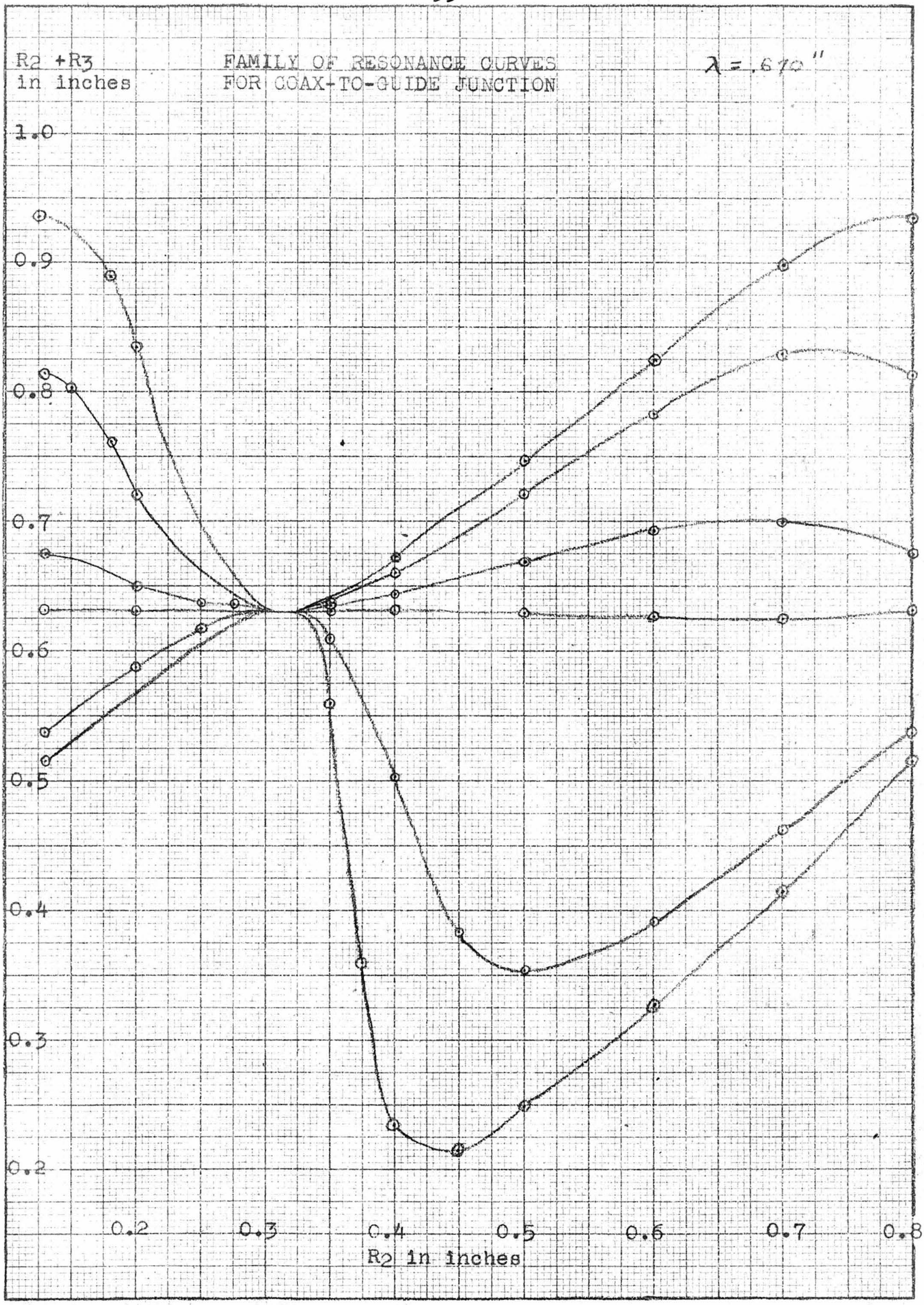
R2 +R3
in inches
FAMILY OF RESONANCE CURVES
FOR COAX-TO-GUIDE JUNCTION
λ = .670"
1.0
0.9
0.8
0.7
0.6
0.5
0.4
0.3
0.2
0.2
0.3
0.4
0.5
0.6
0.7
0.8
R2 in inches

Fig. 21

guide arm.*

If the guide arms, say, are fixed and the resonance curve, using just the coax arms, obtained, the junction should appear to be a simple T-section. If a family of such curves is obtained, the T-sections should all have the same series arms. But we have seen (p. 12) that this means the curves must all have a common point as either a maximum or a minimum. Such a family of curves is shown in Fig. 21. This gives a unique determination of X_2, the coax series arm. Repeating the same process, except with the coax arms fixed, and taking resonance curves with the guide arms, we obtain a similar set of curves and thus determine X_1, the guide series impedance.

To complete our measurements, we will take a resonance curve, keeping the two coax arms terminated the same, and the two guide arms terminated the same. The equivalent circuit under these conditions reduces to Fig. 22 where:

$$\begin{aligned} X_1' &= X_1 + 2X_3 \\ X_2' &= X_2 + 2X_4 \\ X_3' &= 2X_5 \end{aligned} \qquad (48)$$

---

* If we should know the two characteristic impedances, as for instance in the junction formed by two different coax lines passing through each other, then the five impedances (starred) are related to the dimensionless ones above by:

$$X_1 = \frac{X_1^*}{Z_{K1}}\ ; \quad X_2 = \frac{X_2^*}{Z_{K2}}\ ; \quad X_3 = \frac{X_3^* + X_5^*}{Z_{K1}} - \frac{X_5^*}{\sqrt{Z_{K1} Z_{K2}}}\ ;$$

$$X_4 = \frac{X_4^* + X_5^*}{Z_{K2}} - \frac{X_5^*}{\sqrt{Z_{K1} Z_{K2}}}\ ; \quad X_5 = \frac{X_5^*}{\sqrt{Z_{K1} Z_{K2}}}\ .$$

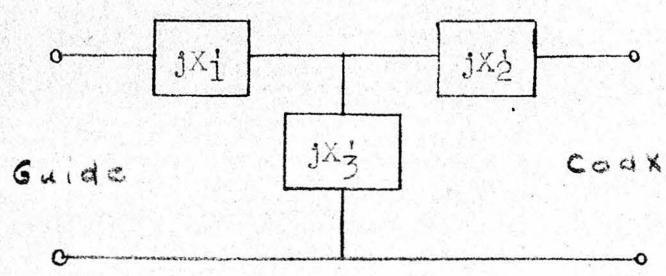

Fig. 22

On p.13, we found the region of measurement which gives minimum error for a symmetrical section. The similar attack for the asymmetrical section is very much more complicated. We should not go too far wrong, however, if we add a length of line ϑ to one side of the T-section and subtract it from the other so as to make the sections symmetrical, measure the symmetrical section at its region of minimum error, and transform the results back to the original asymmetrical section. The transformations are obtained by equating coefficients in the resonant equations for the two sections.

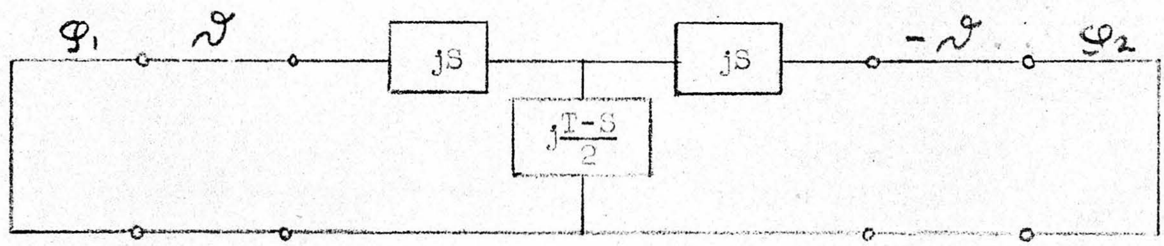

Fig. 23

The resonant equation for Fig. 23 is:

$$\frac{1}{\tan(\varphi_1+\vartheta)+S}+\frac{1}{\tan(\varphi_2-\vartheta)+S}+\frac{2}{T-S}=0 \tag{49}$$

or writing $\quad \phi=\tan\varphi \quad , \quad \Theta=\tan\vartheta$

$$\phi_1\phi_2+\frac{(T+S)(1+\Theta^2)-2\Theta(1+TS)}{2-2TS\Theta^2}\phi_1$$

$$+\frac{(T+S)(1+\Theta^2)+2\Theta(1+TS)}{2-2TS\Theta^2}\phi_2+\frac{TS-\Theta^2}{1-TS\Theta^2}=0 \tag{50}$$

When shorted lines are added to Fig. 22 to form a cavity, we have: $\quad \dfrac{1}{\phi_1+X_1'}+\dfrac{1}{\phi_2+X_2'}+\dfrac{1}{X_3'}=0$

or

$$\phi_1\phi_2+(X_2'+X_3')\phi_1+(X_1'+X_3')\phi_2+X_1'X_2'+X_2'X_3'+X_3'X_1'=0 \tag{51}$$

Equating coefficients of ϕ's in Eqs. 50 and 51 and solving, we get:*

$$X_1'=\frac{S(1+\Theta^2)+\Theta(1+TS)}{1-TS\Theta^2} \tag{52a}$$

$$X_2'=\frac{S(1+\Theta^2)-\Theta(1+TS)}{1-TS\Theta^2} \tag{52b}$$

$$X_3'=\frac{(T-S)(1+\Theta^2)}{2(1-TS\Theta^2)} \tag{52c}$$

---

* Interchanging T and S gives solutions also; we have chosen the above because when $\Theta\to 0$, $X_1'\to X_2'\to S$ and $X_3'\to \frac{T-S}{2}$.

Numerical Results of Measurements On a Coax-to-Guide Junction

Figs. 24 and 25 show the resonant cavity used for measuring the equivalent circuit of the coax-to-guide junction. The inner conductor of the coax line is part of one plunger and slides inside the other plunger. All sliding contacts were fitted with spring fingers one-quarter wavelength long enabling the contact to occur at a current minimum. Although the machining was held to very close tolerances, the cavity did not function as well as it was hoped it would. The half wavelength varied by as much as

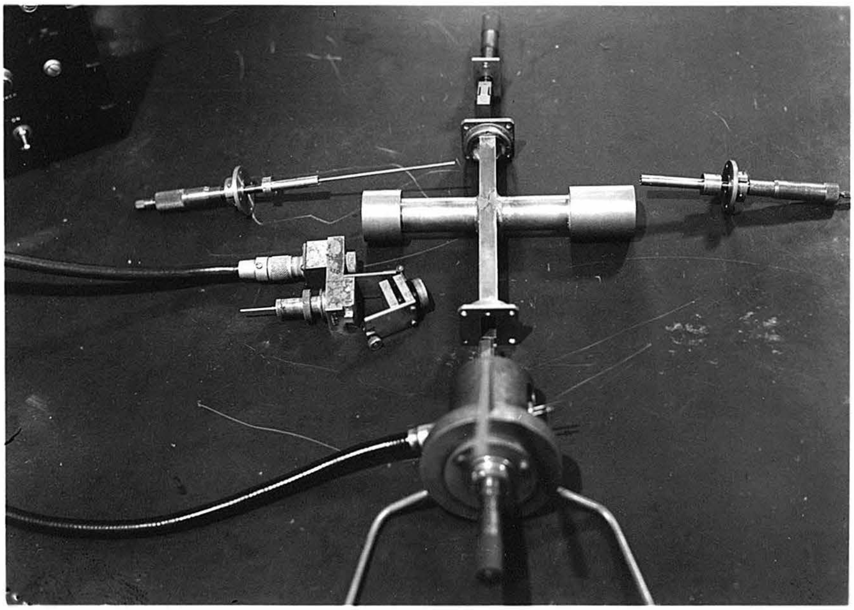

Fig. 24

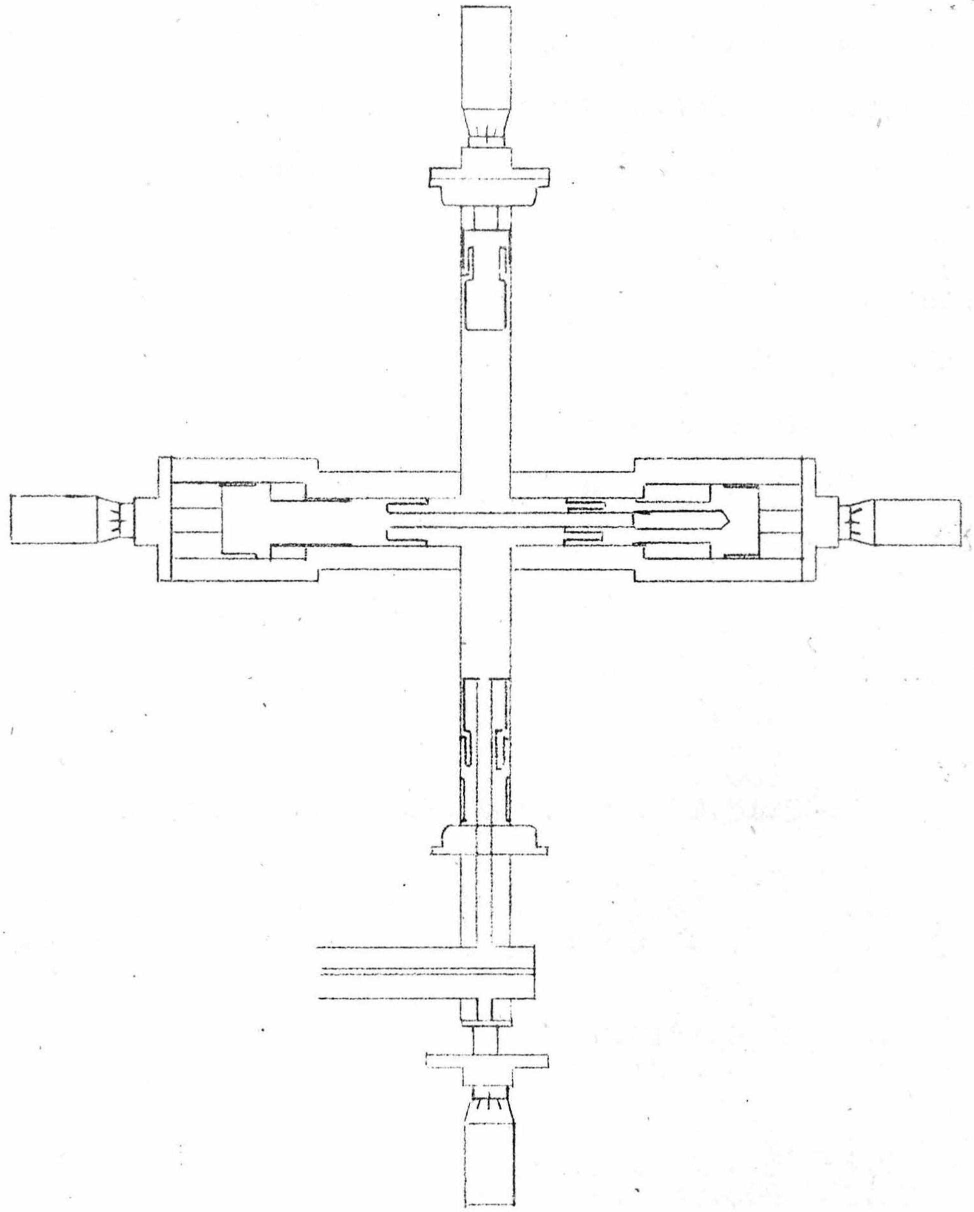

Fig. 25

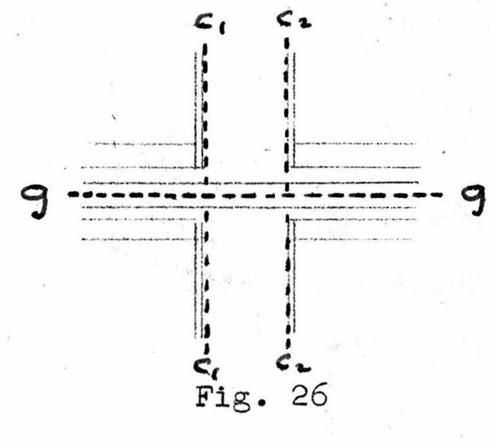

Fig. 26

0.005 inches from its theoretical value of 0.669 inches. This was probably due to small lateral motion of the inner conductor where it crossed the guide. Two sets of coax plungers having different inner conductor diameters were made. The results of these measurements are given in Table III. The reference planes for the guide arms are coincident with the axis of the coax line. The reference planes for the coax arms are flush with the inside of the guide. (See Fig. 26.)

Guide Width	0.900 "	
Guide Height	0.402 "	
λ_{air}	3.403 cm	
λ_g	2.006 "	
Diameter of Outer Coax Conductor	0.3125"	
Diameter of Inner Coax Conductor	0.136"	0.0945"
Coax Z_k	49.9 Ω	71.8 Ω
X_1	-0.016 ±.001	0.012 ±.001
X_2	-1.15 ±.01	-0.99 ±.01
S	-0.158 ±.001	-0.051 ±.001
T	-3.056 ±.003	-3.021 ±.003
θ	0.953 ±.005	1.299 ±.005
X_3	1.00 ±.01	0.90 ±.01
X_4	-0.95 ±.01	-0.60 ±.01
X_5	-2.46 ±.02	-2.60 ±.02

TABLE III

The errors in X_1 , X_2 , S , T and θ were estimated from the curves used to determine them. The errors in X_3 , X_4 and X_5 were computed from the errors in S, T and θ using the partial derivative of X_3 , X_4 and X_5 with respect to S, T and θ . The values in Table III were checked using the resonance equation for Fig. 20:

$$\frac{1}{jX_3+\cfrac{1}{\cfrac{1}{jX_1+j\tan\beta_1 l_1}+\cfrac{1}{jX_1+j\tan\beta_1 l_4}}}+\frac{1}{jX_4+\cfrac{1}{\cfrac{1}{jX_2+j\tan\beta_2 l_2}+\cfrac{1}{jX_2+j\tan\beta_2 l_3}}}+\frac{1}{jX_5}=0$$

Additional data not used in the original computation of the X's was checked, assuming three of the l's and computing the fourth. In every case the measured values of the l's agreed with the computed values within a few thousandths of an inch. Two sets of values for X_3 , X_4 and X_5 can be computed, depending on whether S or T is associated with the maximum of the resonance curve. The two sets of values give the same resonant behavior, but one of them has the phases in the coax arms shifted 180° with respect to the other. The alternative values are given in Table IIIa:

Coax Z_K	49.9 Ω	71.8 Ω
S	-3.056	-3.021
T	-0.158	-0.051
θ	0.953	1.299
X_3	-3.94	-4.37
X_4	-5.86	-6.44
X_5	2.46	2.60

TABLE IIIa

Description of Automatic Frequency Control System

In order to obtain accuracy in a cavity containing several wavelengths, it is necessary that the frequency be held very constant. The system shown in Figs. 27 and 28 was designed with this in mind. The 419-B klystron was immersed in a water-cooled oil bath. The frequency of the reflex klystron being very dependent on the reflector voltage, an automatic frequency control feature was incorporated by feeding a large fraction of the output through a cavity so that the operating frequency was on the steep portion of its resonance curve. From the cavity it was taken across high

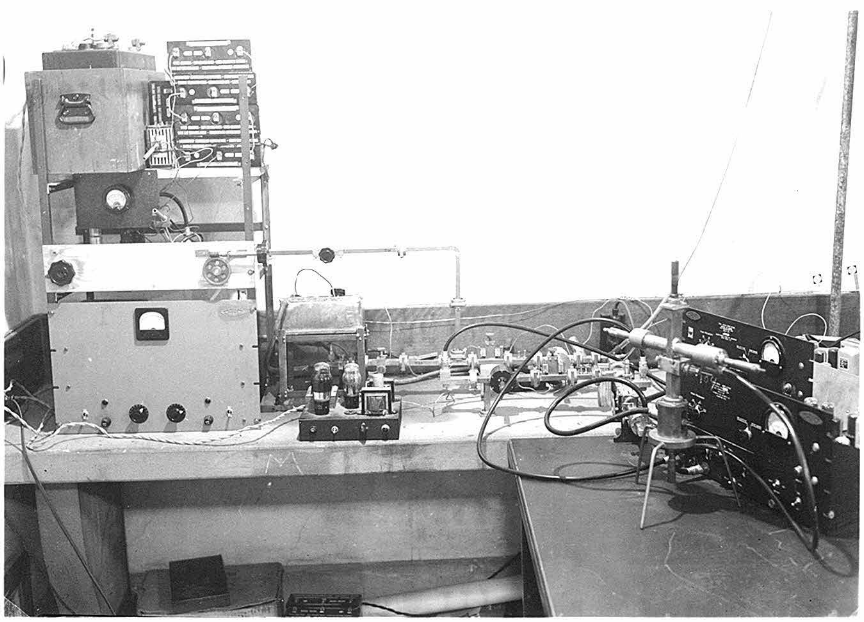

Fig. 27

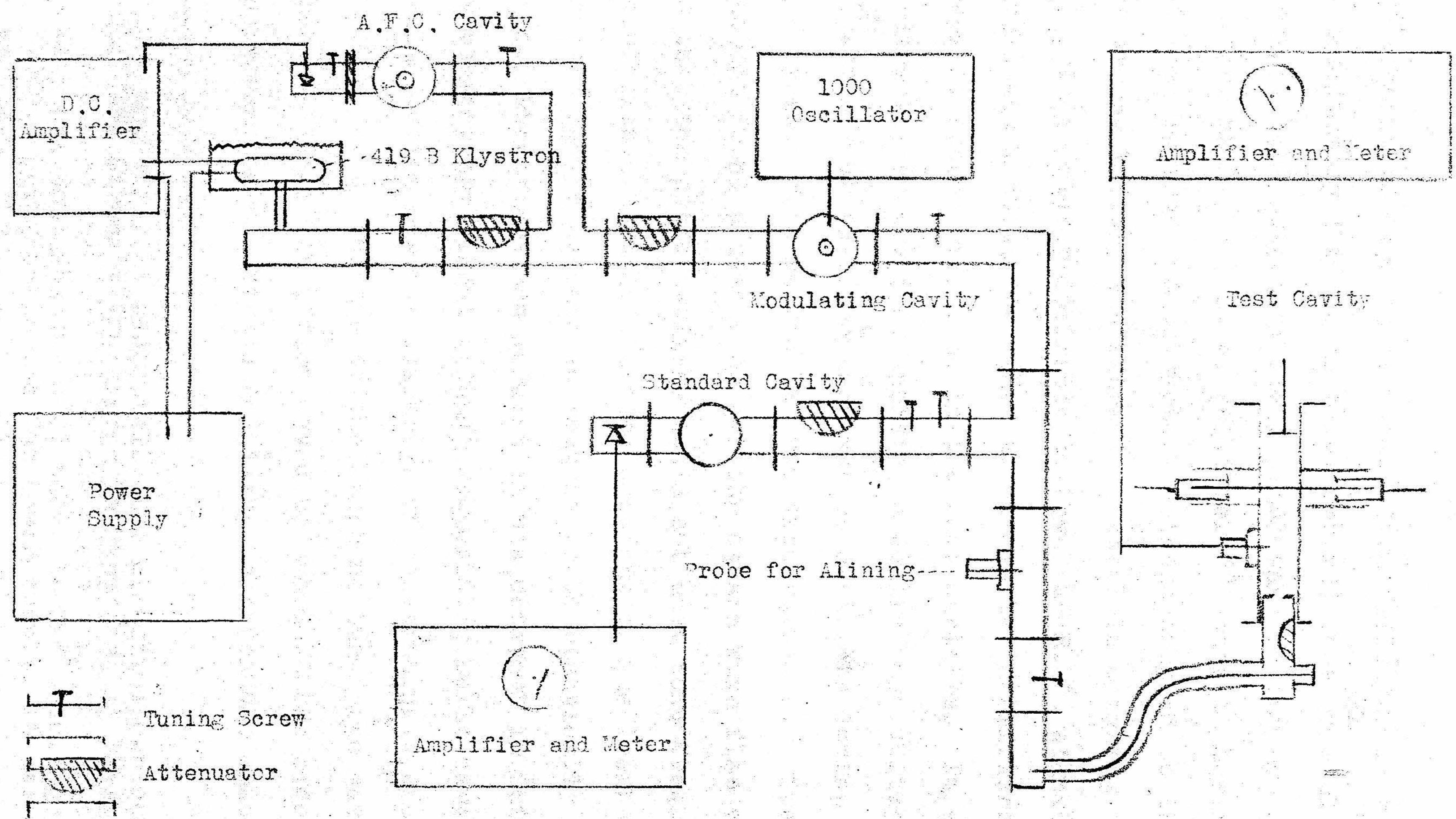

SCHEMATIC DIAGRAM OF PRECISION AUTOMATIC FREQUENCY CONTROL SYSTEM

Fig. 28

voltage insulation in the guide (the reflector is at approximately 1200 volts below ground) to a crystal detector. The output of the crystal was fed through a stable, high gain, d. c. amplifier *[4] back to the reflector of the klystron. A voltmeter, cathode-coupled to the output of the amplifier, was extremely useful in aligning the system.

It is highly desirable to have the R. F. signal purely amplitude modulated so that a. c. coupled amplifiers may be used to detect resonance in the test cavities. This is ordinarily achieved by applying a square wave voltage to the klystron such that the tube cannot oscillate during half the cycle. This method has two disadvantages. First, it was not found possible to get the square wave flat enough so that the output voltage would not have some frequency modulation. Second, the time constant of the feedback circuit had to be made so long as to be practically useless. Pure amplitude modulation was obtained in this case by passing the signal through a specially built cavity, one wall of which was the diaphragm of an earphone. Applying a 1,000 c. p. s. voltage to the earphone tuned the cavity so that the signal in effect moved up and down the side of its resonance curve. It was necessary to attenuate considerably

---

* The amplifier is essentially the circuit shown on p. 429 of John Strong's Procedures in Experimental Physics, which uses one pentode as the plate load for another. With one 6SH7 and one 6SJ7 tube, it had a voltage gain of 4,000. Using batteries for power supply, it was extremely stable.

between the klystron and the modulating cavity so that the klystron's load would appear constant. The guide from the modulating cavity branched, one arm going to a high Q, invar steel, standard cavity, which was constantly monitored, and the other to the test cavity. When operating at its best, the frequency did not deviate noticeably from the peak of the standard cavity, the Q of which was around 40,000, during periods of half an hour or so. Measurements were taken when the system was considered to be drifting rather badly, and the drift was about one part in 200,000 per minute and very constant throughout the half-hour period the measurement occupied.

Example of Precision Measurement

To illustrate the precision obtainable with such a system, we give here data comparing the wavelength measured in a carefully broached and lapped section of brass wave-guide and the wavelength as measured in two coax wavemeters.

Wavelength in guide.

Average measured λ_g = 2.00585" $\pm 3.0 \times 10^{-5}$ *
Guide width ** = 0.89986" $\pm 3.9 \times 10^{-5}$
λ_c = 1.79972" $\pm 7.8 \times 10^{-5}$

---

* Here and in the following, the values given after the ± signs are standard deviations (σ), not probable errors.

** See Appendix A.

Substituting in $$\frac{1}{\lambda^2} = \frac{1}{\lambda_g^2} + \frac{1}{\lambda_c^2}$$

gives: $$\lambda/2 = 1.7013 \pm 6 \times 10^{-5} \text{ cm}$$

Coax Wavemeters.

Wavemeter A
Salisbury Coax Wavemeter
Mico Instrument Co. #454

Wavemeter B
Mico Instrument Co. Cat. No. 402-A, Serial No. 2327

Wavemeter A contained 10 resonant peaks of the principal mode ranging from 5 to 14 half wavelengths. It is possible to repeat the settings of the wavemeter more closely than the scale could be read (0.001 cm). The data was fitted by the method of least squares to the equation:

$$r_n = a + n\lambda/2 \tag{53}$$

giving:

Run	a	$\lambda/2$
I	-0.0129 cm	$1.70138 \pm 1.1 \times 10^{-4}$ cm
II	0.0087 cm	$1.70138 \pm 9 \times 10^{-5}$ cm

The close agreement in the $\lambda/2$'s is probably fortuitous. However, the error was not purely random. Although the two runs were made 3 weeks apart, the residuals appeared to be a periodic function of position in the wavemeter and had a rank-difference coefficient of correlation of 0.81.

Wavemeter B contained 5 resonant peaks ranging from 3 to 7 half wavelengths. The least squares fitting gave:

$\lambda/2 = 1.70124 \pm 4.5 \times 10^{-5}$ cm

Wavemeter A also contained the next higher mode, TE_{11}. The wavelength in the wavemeter, λ_w, for this mode is given by:

$$\frac{1}{\lambda_w^2} = \frac{1}{\lambda^2} - \frac{1}{\lambda_c^2} \quad \text{where} \quad \lambda_c = \frac{2\pi a}{x_{11}}$$

x_{11} being the first root of the equation

$$J_1'(x_{1m})\, Y_1'\!\left(\tfrac{b}{a} x_{1m}\right) - J_1'\!\left(\tfrac{b}{a} x_{1m}\right) Y_1'(x_{1m}) = 0 \qquad (54)$$

a being the radius of the inner conductor, b the radius of the outer conductor and k equal to b/a. Appendix B is a table of the first root of Eq. 54 for k's covering the range in which wavemeters are usually built. This range of k occurs in wavemeters which have optimum Q [5].

This mode, however, is not as accurate as the principal mode since the wavelength measured depends upon the radii of the coax line. A close examination of the wavemeter revealed that it was badly scored by the sliding contact and several thousandths of an inch out of round at the places where the legs were fastened. It is seen that the two runs do not agree nearly as well as the principal mode measured at the same time. The least square fitting of the data to Eq. 53 gave:

Run	a	$\lambda/2$
I	0.0398 cm	$1.9685 \pm 1.1 \times 10^{-4}$ cm
II	0.0624 cm	$1.9660 \pm 2.3 \times 10^{-4}$ cm

Again, the errors are not purely random, the residuals having a rank-difference coefficient of correlation of 0.66.

Computing the wavelength in air, λ :

$$
\begin{array}{llll}
a = 0.4009'' & \pm .0005'' & & \\
b = 1.369\ '' & \pm .002\ '' & & \\
k = 3.4148 & \pm .0065 & & \\
x_{11} = 0.46591 & \pm .00068 & & \\
\lambda_c = 6.866 & \pm .026 & \text{cm} & \\
\lambda = \begin{cases} 3.415 \\ 3.413 \end{cases} & \begin{array}{l} \pm .003 \\ \pm .003 \end{array} & \begin{array}{l} \text{cm} \\ \text{cm} \end{array} & \left.\begin{array}{l} \text{Run I} \\ \text{Run II} \end{array}\right\}
\end{array}
$$

The discrepancy here might be caused by the wavelength in the wavemeter being commensurable with the error period in the wavemeter screw. In any event, the higher mode is definitely inferior for precision measurements because of its dependence on transverse dimensions.

APPENDIX A

Note on Internal Wave Guide Measurements

In work of this sort, it is necessary to make mechanical measurements of distances which are often not measurable directly with micrometers. Short pieces of drill rod, which is readily obtainable and accurately ground, are extremely useful. Two examples will be given.

1. Measurement of Guide Width

Fig. 29 shows the setup. A depth micrometer was used to measure the distance $\ell = \ell_1 - \ell_2$, and the radius a was measured with outside micrometers. Although the value of a is very critical, by placing two of the cylinders in contact with their axes at right angles, 4 a was measured with a corresponding reduction in the error in a. Two different

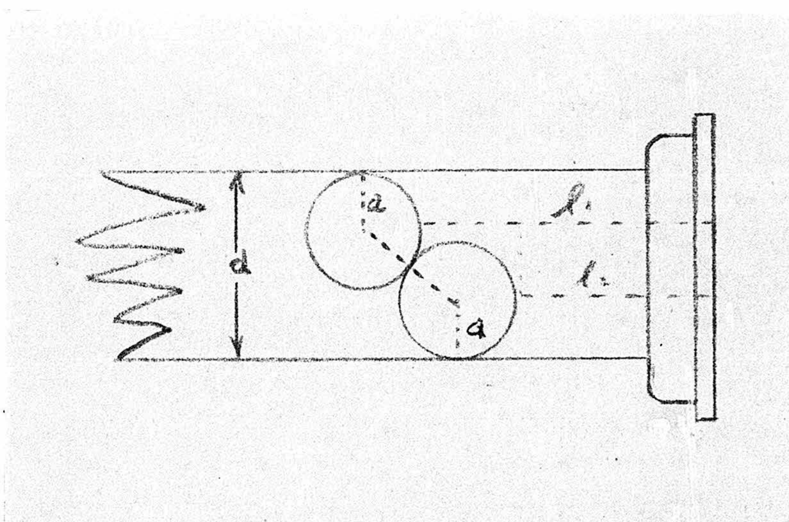

Fig. 29

sizes of drill rod, having nominal radius values of 1/4" and 15/64", were used. Five runs were made, using different cylinders. ℓ was measured 8 times (the cylinders were removed and replaced between measurements), and a was measured 10 times for each run. From Fig. 29:

$$d = 2a + \sqrt{4a^2 - \ell^2}$$

$$\frac{\partial d}{\partial a} = 2 + \frac{4a}{\sqrt{4a^2 - \ell^2}}$$

$$\frac{\partial d}{\partial \ell} = -\frac{\ell}{\sqrt{4a^2 - \ell^2}}$$

$$d = 0.9000''$$

a	ℓ	$\frac{\partial d}{\partial a}$	$\frac{\partial d}{\partial \ell}$
0.2500 "	0.3000 "	4.50	-0.75
0.234375 "	0.18371 "	4.174	-0.426

Typical computation:

$$\ell_{av} = 0.1821'' \pm 1.8 \times 10^{-4} \, ''$$

$$a_{av} = 0.234205'' \pm 2.6 \times 10^{-6} \, ''$$

$$\Delta \ell = 0.1821 - 0.1837 = -0.0016$$

$$\Delta a = 0.234205 - 0.234375 = -0.00017$$

$$d = 0.90000 - 0.00071 + 0.00068$$

$$= 0.89997''$$

$$\sigma_d = \left[(4.2 \times 2.6 \times 10^{-6})^2 + (.43 \times 1.8 \times 10^{-4})^2 \right]^{\frac{1}{2}}$$

$$= 7.8 \times 10^{-5} \, ''$$

The results for 5 runs were:

0.89997 0.89999 0.89989 0.89963 0.89990

giving:

$$d_{av} = 0.89986 \, ''$$

$$\sigma_{d_{av}} = 3.9 \times 10^{-5} \, ''$$

2. Measurement of 60-Degree H-Plane Corner

It is necessary to know the distances of the reference planes of the corner from the ends. These measurements are made with the arrangement shown in Fig. 30. A cylinder was placed in the corner and two parallel blocks of steel, sliding smoothly in the guide, were placed one in each arm. Readings were taken on the two micrometers and their sum plotted against one of them to give the curve shown in Fig. 31.

The slope of the curves (shown dotted) can be calculated from θ. The curves intersect when the cylinder touches

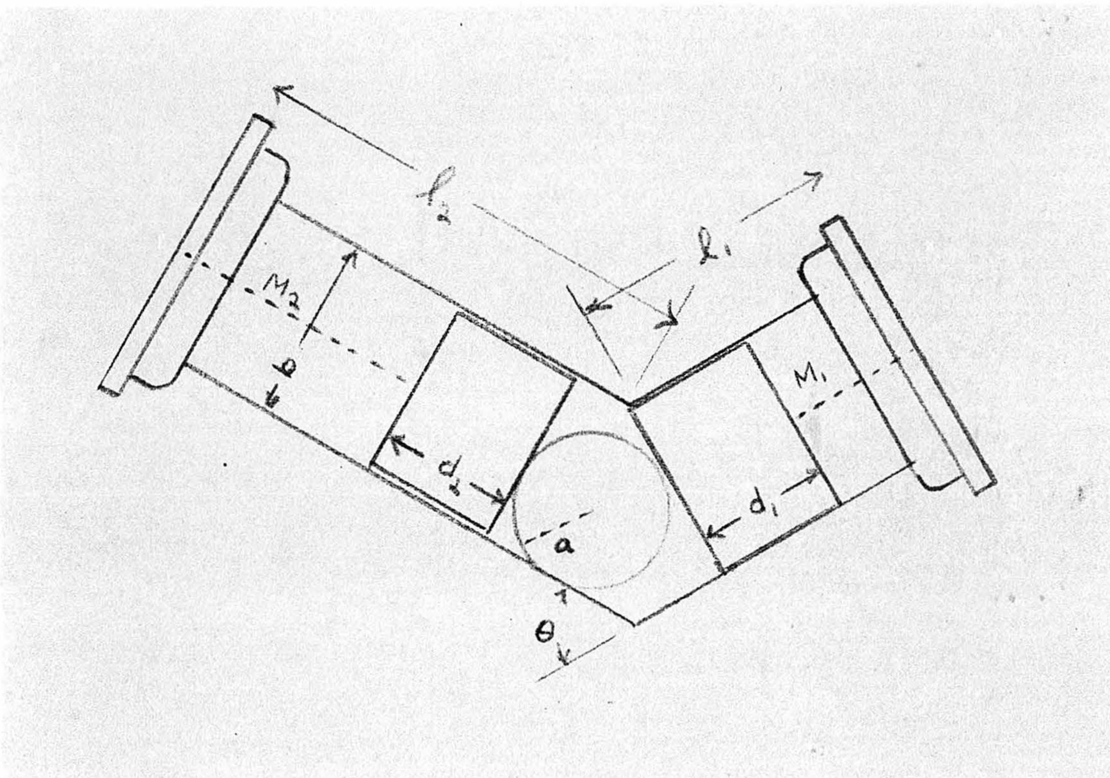

Fig. 30

both guide walls; in this example this occurs when $M_2 = 3.1837''$ and $M_1 = 3.4682 - 3.1837 = 0.2845.''$ Then:

$$\ell_1 = 0.2845 + d_1 + a - (b - a)\cot\frac{\theta}{2}$$

$$\ell_2 = 3.1837 + d_2 + a - (b - a)\cot\frac{\theta}{2}$$

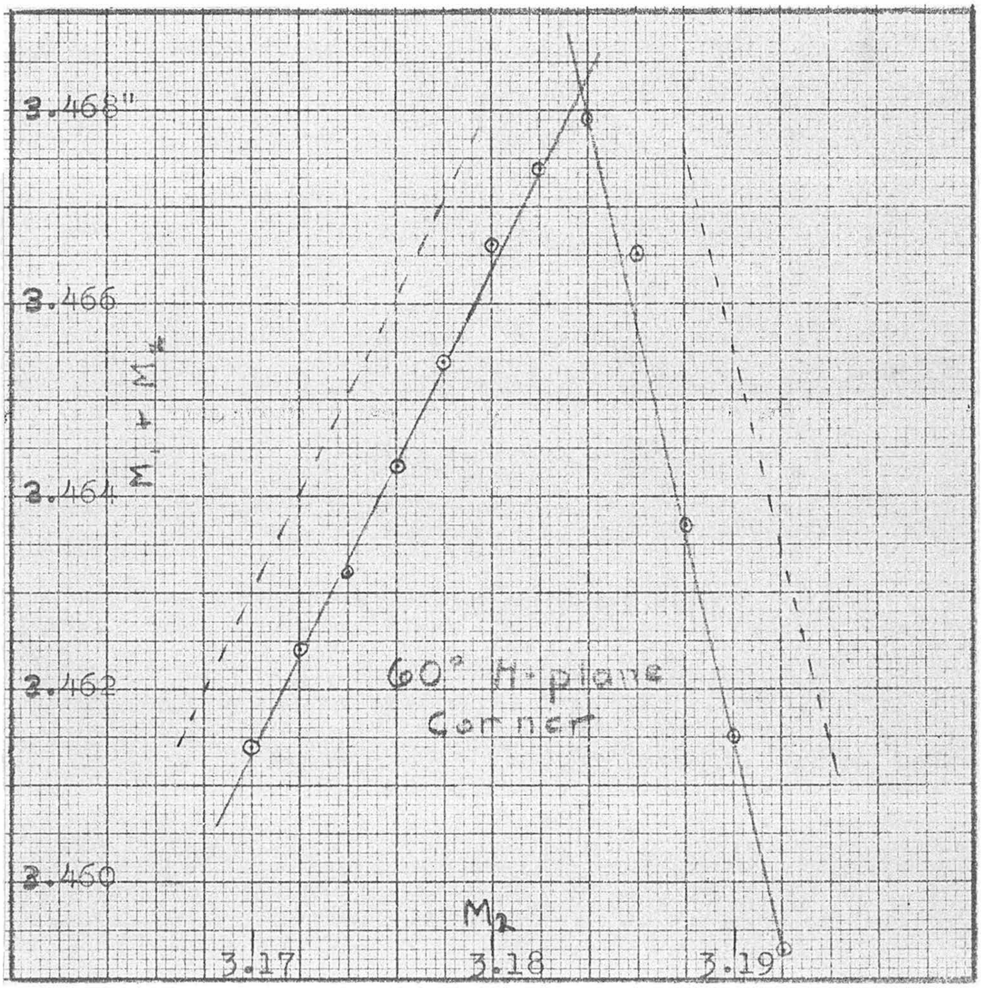

Fig. 31

APPENDIX B

First Root of the Equation $J_1'(x)\,Y_1'(kx) - J_1'(kx)\,Y_1'(x) = 0$ As a Function of k for Values of k in the Region Which Gives Maximum Q When Used in Coaxial Lines

x	k	Δk	(k+1)x	Δ(k+1)x
.44	3.67478		2.05690	
		.10345		-20
.45	3.57133		2.05710	
		.09960		10
.46	3.47173		2.05700	
		.09553		19
.47	3.37620		2.05681	
		.09183		31
.48	3.28437		2.05650	
		.08837		46
.49	3.19600		2.05604	
		.08~~6~~07		58
.50	3.11093	5	2.05546	

The function (k+1)x is tabulated as an aid to interpolation.

Method of Computation

Rough values of k and x were taken from a curve given by R. Truell.[6] Values of $J_1'(x)/Y_1'(x)$, $(.44 \leq x \leq .50)$ and $J_1'(kx)/Y_1'(kx)$ $(1.57 \leq kx \leq 1.63)$ were obtained for .01 increments of the argument from tabulations of $J_0(x)$, $J_1(x)$, $Y_0(x)$ and $Y_1(x)$ [7] using the equations:

$$J_1'(x) = J_0(x) - \frac{1}{x} J_1(x)$$

$$Y_1'(x) = Y_0(x) - \frac{1}{x} Y_1(x)$$

Exact values of kx were obtained by matching the second set of values $J_1'(kx)/Y_1'(kx)$ to the first $J_1'(x)/Y_1'(x)$, using the method of divided differences [8] for the inverse interpolation.

APPENDIX C

Transmission and Reflection Coefficients of a T-Section Inserted in an Infinite Line

If in Fig. 2 (p. 3) $V(x)$ is the voltage across the line and I_x is the current along the line, where x is measured from the terminals of the T-section, then the following equations [9] hold (omitting the time variation term):

$$\left.\begin{aligned} I &= A e^{-j\beta x} + B e^{j\beta x} \\ V &= A e^{-j\beta x} - B e^{j\beta x} \end{aligned}\right\} \quad x < 0$$

$$\left.\begin{aligned} I &= C e^{-j\beta x} \\ V &= C e^{-j\beta x} \end{aligned}\right\} \quad x > 0$$

Applying ordinary circuit theory to the T-section gives:

$$\tfrac{1}{2}\, j\,(T + S)(A + B) - \tfrac{1}{2}\, j\,(T - S)\,C = A - B$$

$$\tfrac{1}{2}\, j\,(T - S)(A + B) - \tfrac{1}{2}\, j\,(T + S)\,C = C$$

Solving for the reflection and transmission coefficients,

$$\frac{B}{A} = \frac{1 + TS}{1 - TS + j(T + S)} \tag{55}$$

$$\frac{C}{A} = \frac{j\,(T - S)}{1 - TS + j\,(T + S)} \tag{56}$$

Letting

$$T = \tan t \qquad S = \tan s \tag{8}$$

we obtain:

$$\frac{B}{A} = \cos(s-t)\, e^{-j(s+t)} \tag{6}$$

$$\frac{C}{A} = -j \sin(s-t)\, e^{-j(s+t)} \tag{7}$$

APPENDIX D

Reflection Coefficient Due to Two Symmetrical T-Sections Inserted in an Infinite Line a Distance L Apart

Consider the discontinuities, (1) and (2), in Fig. 32, represented by two different symmetrical T-sections separated by a distance of L.

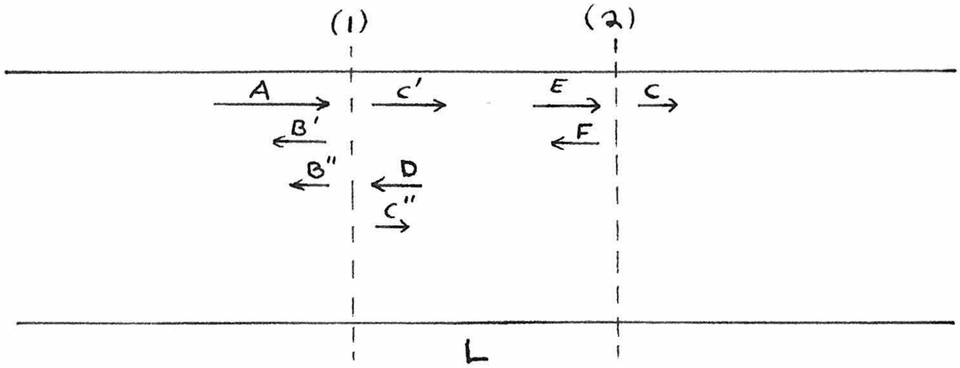

Fig. 32

A wave of amplitude A advances from the left and is reflected B', and transmitted C'. Because of reflections from (2), there will be a wave D advancing on (1) from the right, which is transmitted B" and reflected C". But the wave hitting (2) from the left is just C'+ C", with its phase retarded because of the distance L. Likewise, D is just the reflected wave F retarded by a similar phase change.

Analysis of each group separately:

A, B', C'

$$B' = A\cos(s_1 - t_1)\, e^{-j(s_1+t_1)}$$

$$C' = -jA\sin(s_1 - t_1)\, e^{-j(s_1+t_1)}$$

D, B", C"

$$C'' = D\cos(s_1 - t_1)\, e^{-j(s_1+t_1)}$$

$$B'' = -jD\sin(s_1 - t_1)\, e^{-j(s_1+t_1)}$$

E, F, C

$$F = E\cos(s_2 - t_2)\, e^{-j(s_2+t_2)}$$

Phase shift due to travel on line having $Z_K = 1$, $\gamma = j\beta$

$$E = (C' + C'')\, e^{-j\beta L}$$

$$D = F e^{-j\beta L}$$

Net reflection coefficient

$$B = B' + B'' = \text{net reflected wave}$$

$$B = A\cos(s_1 - t_1)\, e^{-j(s_1+t_1)} - jD\sin(s_1 - t_1)\, e^{-j(s_1+t_1)}$$

$$C' + C'' = -jA\sin(s_1 - t_1)\, e^{-j(s_1+t_1)} + D\cos(s_1 - t_1)\, e^{-j(s_1+t_1)}$$

$$De^{j\beta L} = \cos(s_2 - t_2)\, e^{-j(s_2+t_2)}\,(C' + C'')\, e^{-j\beta L}$$

Eliminating C'+ C" and D gives

$$\frac{B}{A} = \frac{\cos(s_1 - t_1)\, e^{-j(s_1+t_1)} - \cos(s_2 - t_2)\, e^{-j[s_2+t_2+2(s_1+t_1)+2\beta L]}}{1 - \cos(s_1 - t_1)\cos(s_2 - t_2)\, e^{-j(s_1+t_1+s_2+t_2+2\beta L)}} \qquad (10)$$

GLOSSARY OF SYMBOLS

α	$\dfrac{\vartheta_1 + \vartheta_2}{2}$
A	$\tan\alpha$ (p. 12 only)
β'	$\dfrac{\vartheta_1 - \vartheta_2}{2}$
B	$\tan\beta'$ (p. 12 only)
β	imaginary part of propagation constant, equal to $2\pi/\lambda_g$
γ	propagation constant of a transmission line, equal to $j\beta$ for a lossless line
Γ	propagation constant of a T-section
δ, ϵ	small quantities
ϑ	βl_0
θ	$\tan\vartheta$
λ	wavelength in free space
λ_c	cutoff wavelength
λ_g	wavelength in guide
λ_w	wavelength in wavemeter
σ	standard deviation
ϑ_i	βl_i
ϕ_i	$\tan\vartheta_i$
Ω	ohms
a	radius of inner conductor of coax line. Radius of cylinder. Also used to designate a particular section of wave guide as distinct from guide <u>b</u>
A	complex amplitude of wave advancing on an obstacle inserted in an infinite line

b	radius of outer coax conductor
B	complex amplitude of wave reflected by an obstacle inserted in an infinite line
c.p.s.	cycles per second
C	complex amplitude of wave transmitted by an obstacle inserted in an infinite line
d	distance. In particular, the width of a rectangular wave guide
E_i	voltage across the i^{th} pair of terminals of a network
I_i	current flowing to and from the i^{th} pair of terminals
$I(x)$	current flowing at the point x on a transmission line
j	$\sqrt{-1}$
J_1'	derivative of the Bessel function of the first kind, order one, with respect to its argument
k	ratio of the outer to inner conductor radii of a coax line b/a
ℓ	length
ℓ_i	length of the i^{th} shortcircuited line forming part of a cavity
ℓ_0	length of line that must be added to one side of an asymmetrical T-section and subtracted from the other side in order that it may appear symmetrical
L	distance between the reference planes of two obstacles on the same transmission line
m,n,p	integers or zero
Q	figure of merit, the ratio of energy stored per cycle to energy dissipated per cycle

r_n — n^{th} wavemeter scale reading

R — micrometer readings (p. 16 only). Purely resistive characteristic impedance of a transmission line (pp. 25, 26)

s — $\tan^{-1} S$

S — dimensionless series impedance of symmetrical T-section (Fig. 1b, p. 2)

S.W.R. — voltage standing wave ratio

t — $\tan^{-1} T$

T — other dimensionless impedance of symmetrical canonical T-section (Fig. 1b, p. 2)

$V(x)$ — voltage across a transmission line at the point $\underline{x}$

x — distance along transmission line measured from T-section terminals. Also root of Eq. 54

X — purely reactive impedance, dimensionless unless otherwise stated. Components of various equivalent circuits

Y_1' — derivative of Bessel function of the second kind, order one, with respect to its argument, also known as N_1'

Z_k — characteristic impedance of a transmission line or T-section

Z_{oc} — input impedance of a T-section with the output opencircuited

Z_r — impedance terminating a length of line

Z_{sc} — input impedance of a T-section with the output shortcircuited

Z_{ik} — mutual impedance between the i^{th} voltage and the k^{th} current in a multi-terminal network. (Self impedance if $i = k$)

BIBLIOGRAPHY

1 David S. Saxon, "Memorandum on Schwinger's Lectures on Wave Guide Theory."

2 S. C. Snowdon and D. W. Hagelbarger, "A New and Practical Method for Matching Two Obstacles in a Wave Guide." NDRC Div. 14, Report 461, July 1945.

3 W. H. Pickering, D. W. Hagelbarger, C. Y. Meng and S. C. Snowdon, "A New Method for the Precision Measurement of Wave Guide Discontinuities." NDRC Div. 14, Report 317, October 1944.

4 John Strong, "Procedures in Experimental Physics," p. 429. Prentice-Hall, Inc., New York.

5 Terman, "Radio Engineers Handbook," p. 192. McGraw-Hill, 1945.

6 R. Truell, "Concerning the Roots of $J_n'(x) N_n'(kx) - J_n'(kx) N_n'(x) = 0$." J. Appl. Phys., Vol. 14, pp. 350-52, July 1943.

7 "Bessel Functions Part I, Functions of Orders Zero and Unity." British Assoc. Math. Tables, Vol. VI, Cambridge, 1937.

8 See Milne, "Numerical Calculus," or Whittaker and Robinson, "Calculus of Observation."

9 J. C. Slater, "Microwave Transmission," pp. 23-4. McGraw-Hill, 1942.